Article

Crystal Engineering of Tegafur Cocrystals: Structural Analysis and Physicochemical Properties

Srinivasulu Aitipamula, Pui Shan Chow, and Reginald B. H. Tan

Cryst. Growth Des., **Just Accepted Manuscript** • DOI: 10.1021/cg501469r • Publication Date (Web): 03 Nov 2014

Crystal Engineering of Tegafur Cocrystals: Structural Analysis and Physicochemical Properties

Srinivasulu Aitipamula,[*†] *Pui Shan Chow,*[†] *and Reginald B. H. Tan*[*†,‡]

[†]Crystallization and Particle Science, Institute of Chemical and Engineering Sciences, A*STAR (Agency for Science, Technology and Research), 1 Pesek Road, Jurong Island, Singapore, 627833. E-mail: srinivasulu_aitipamula@ices.a-star.edu.sg

[‡]Department of Chemical & Biomolecular Engineering, National University of Singapore, 4, Engineering Drive 4, Singapore 117576. E-mail: reginald_tan@ices.a-star.edu.sg

ABSTRACT. Tegafur (TG) is a chemotherapy agent and has been used in the treatment of several common cancerous tumors. Despite wide utility of TG as a main component of the TG-uracil combination drug, TG suffers severe drawbacks due to non-uniform oral absorption, a short biological half-life, and poor aqueous solubility. We report cocrystals of TG with pharmaceutically acceptable coformers such as nicotinamide, isonicotinamide, 4-hydroxybenzoic acid, pyrogallol and an anti-asthma drug, theophylline. The selection of these coformers was made based on the crystal engineering principles by analyzing the crystal structures in the Cambridge Structural Database. Cocrystals were prepared by conventional solvent evaporative crystallization and solid-state grinding techniques and characterized by FT-IR, thermal analysis and X-ray diffraction techniques. Crystal structure analysis revealed heterosynthons between TG and the coformers in most of the cocrystals. Stability of the cocrystals was tested at accelerated conditions (40 °C, 75 % relative humidity), slurry, and dynamic vapor sorption techniques that revealed greater stability of the cocrystals with isonicotinamide, 4-

hydroxybenzoic acid and theophylline. Solubility and dissolution rate of the TG-isonicotinamide cocrystal were found superior to the other cocrystals and TG, making it a promising cocrystal for development of novel TG formulations.

INTRODUCTION

Arrangement of molecules in three-dimensional crystal lattice determines the properties of solid materials.[1] Therefore, control over crystal packing through manipulation of intermolecular interactions that connect the molecules in the crystal lattice is of paramount importance in an attempt to design a crystal with desired properties. Over the past few decades, crystal engineering has evolved as an incredible tool for predicting possible intermolecular interactions, thereby designing the target crystals.[2-4] Exploiting the crystal engineering strategies will aid in the design of crystals that contain more than one molecule (eg. cocrystals) and the past decade has seen an explosion of interest in the design, synthesis, and development of cocrystals for various applications.[5-9] In pharmaceuticals, cocrystals offer a rational approach to address several important issues in the development of active pharmaceutical ingredients (API).[10-18] For example, cocrystals of APIs (pharmaceutical cocrystals) offer opportunities to modify the properties such as color, stability, solubility, dissolution rate, mechanical properties, and bioavailability.

Tegafur ((RS)-5-Fluoro-1-(tetrahydrofuran-2-yl) pyrimidine-2,4 (1H,3H)-dione, TG, Figure 1) is a chemotherapy agent belonging to the group of nucleoside analogues that has been used clinically for almost 30 years in the treatment of several common cancerous tumors, notably colorectal cancers.[19] TG is also a very effective drug in the treatment of various malignancies, particularly gastrointestinal, bowel, and breast cancers.[20,21] Commercially available TG-uracil (UFUR) combination drug consists

of TG and uracil in a 4:1 molar ratio.[22] TG, being a prodrug, rapidly metabolizes to 5-flurouracil in the liver following intestinal absorption.[23] A recent pharmacokinetic study revealed that *R*-isomer of TG is preferentially metabolized to 5-Fluorouracil compared to *S*-isomer *in vitro*, suggesting that the *R*-isomer of TG is the preferred enantiomer for pharmaceutical development.[24] According to world cancer statistics, colorectal cancer is the third most common cancers in the world with nearly 1.4 million new cases diagnosed in 2012.[25] Alongside the wide utility of TG in chemotherapy, TG suffers from severe drawbacks mainly due to non-uniform oral absorption, a short biological half-life due to rapid metabolism, and inability to overcome the development of multi-drug resistance by cancer cells.[20,21] In addition, low solubility of TG necessitates high dose administration that simultaneously leads to severe dose-limiting side effects in patients.[20,21] A plausible way to overcome some of these drawbacks is to co-administer TG with a lipid soluble drug to prolong the time in which TG remains at the target site.[26] Previous efforts to enhance the therapeutic efficiency of TG were based on formulations of TG-loaded chitosan nanoparticles.[27] The technique has been proven effective for higher drug-loading and a sustained drug release profile. Over the years, five polymorphs of TG have been identified (α, β, γ, δ, and ε) and 3 of them have been structurally characterized.[28-35] Among the five known polymorphs, α and β modifications are used for therapeutic purposes. There are no reports on hydrates, solvates, salts, and cocrystals of TG and that has prompted us to screen for a novel solid form that could have an impact on the pharmacokinetic properties of TG. Based on the crystal engineering strategies, a cocrystal screen of TG with several GRAS (generally regarded as safe) compounds (or coformers)[36] was performed. The cocrystal screening resulted in cocrystals with nicotinamide (NA), isonicotinamide (INA), 4-hydroxybenzoic acid (4HBA), and pyrogallol (PG), and a cocrystal monohydrate with theophylline (TP). All the cocrystals were characterized by thermal, spectroscopic, and X-ray diffraction techniques. The stability of the cocrystals was assessed by

performing dynamic vapor sorption (DVS) experiments and stability experiments at accelerated test condition (40 °C, 75 % relative humidity (RH)). In addition, solubility and dissolution experiments were conducted in pH 6.8 phosphate buffer medium to evaluate the effect of different coformers on the solubility and dissolution rate of TG.

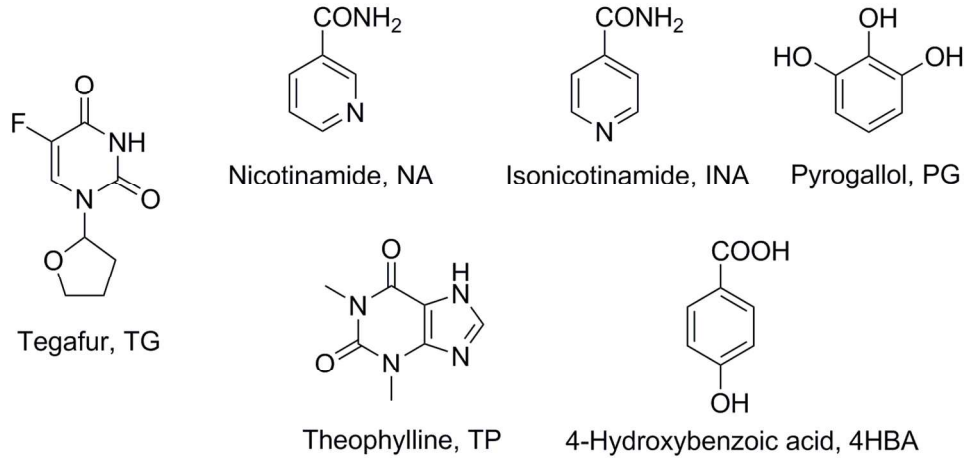

Figure 1. Molecular structure of TG and coformers that formed cocrystals reported in this paper.

RESULTS AND DISCUSSION

Crystal engineering takes the center stage in the design of cocrystals that helps to select suitable coformers for the construction of cocrystals with predictable hydrogen bonding interactions. From a crystal engineering viewpoint, TG represents an interesting and challenging compound for cocrystal design because of the presence of multiple hydrogen bonding sites on the pyrimidinedione ring (Figure 1). TG molecules in the reported polymorphs form cyclic imide-imide dimers (synthon I, Figure 2) involving *R*- and *S*-conformers mediated by N–H···O hydrogen bonds.[28-30] However, the hydrogen bond synthons are entirely different from one polymorph to the other. For example, α-form contains

two symmetry independent molecules and both form synthon I mediated by N1–H···O2 hydrogen bonds (see Figure 2 for atom numbering) (CSD REFCODE: BIPDEJ01),[28] but the synthon I in β-form is mediated by N1–H···O1 hydrogen bond (BIPDEJ02).[29] Interestingly, ε-form, which also has two symmetry independent molecules in the asymmetric unit, features both types of synthons observed in α- and β-forms mediated by N1–H···O2 and N1–H···O1 hydrogen bonds (BIPDEJ03).[30]

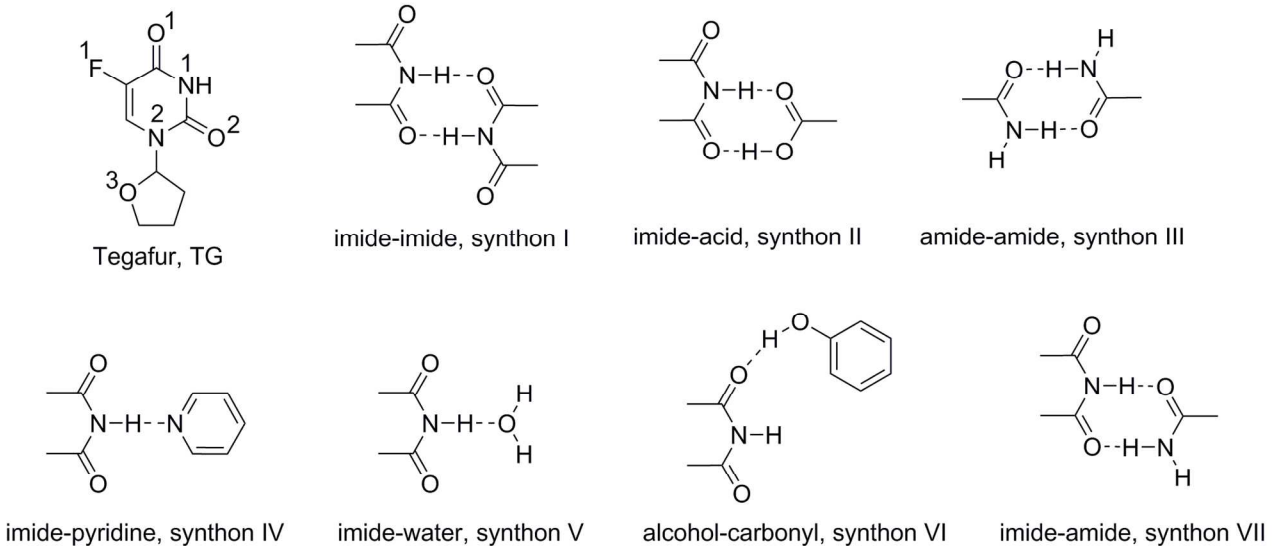

Figure 2. Some observed/plausible supramolecular synthons in the cocrystals of TG.

Supramolecular synthon approach facilitates cocrystal design through wise selection of complementary coformers which can form predictable supramolecular synthons.[37] Statistical analysis of the crystal structures deposited in the Cambridge Structural Database (CSD) serves as a basis for the cocrystal design. The –CO–NH–CO– moiety is one of the prominent functional groups found in many important APIs and nucleosides. For example, barbiturates, lenalidomide, troglitazone, zidovudine, nitrofurantoin, uridine, xanthosine, etc. all feature this functional group. A search for the reported non-ionic crystal structures in the CSD that contain –CO–NH–CO– moiety resulted in a total of 1822 crystal structures that involve cocrystals, solvates and hydrates.[38] All the crystal structures retrieved

from the CSD were carefully analyzed to identify recurring supramolecular synthons. These statistics are summarized in Table 1 and some of the findings are as follows: (a) imide-imide synthon (synthon I) is the prominent synthon in this family of crystal structures which was found in 38 % of the total crystal structures, (b) carbonyl of the –CO–NH–CO– moiety involves in the O–H···O hydrogen bond (synthon VI) with a hydroxyl group in 63 % of the crystal structures in which the two moieties are present together, (c) N–H of the –CO–NH–CO– moiety forms N–H···O hydrogen bond (synthon V) with the O of the water molecule in 30 % of the hydrates, (d) of the 85 crystal structures that contain both pyridyl group and –CO–NH–CO– moieties, 53 % of the crystal structures feature N–H···N hydrogen bond (synthon IV) between N–H of the –CO–NH–CO– moiety and N of the pyridyl group, (e) 87 % of the crystal structures that contain primary amide and –CO–NH–CO– moieties feature $N–H_{amide}\cdots O_{imide}$ hydrogen bond. The above statistics suggest that the imide-imide synthon (synthon I) is the dominant synthon in this family of crystal structures. Therefore, if one were to make a cocrystal of TG, a plausible cocrystal design strategy would be to exploit the –CO–NH–CO– moiety to identify coformers containing a complementary functional group that could preferentially interrupt the imide-imide synthon in the parent TG. The choice of coformers in the present study was made based on the above statistical analysis and pharmaceutical acceptability of the coformers. In particular, the CSD analysis revealed that the coformers that contain hydroxyl (or phenol), amide, and pyridine functionalities could potentially interrupt the imide-imide synthon in the crystal structure of the parent TG and result in a cocrystal. A full list of coformers that were chosen for cocrystal screening with TG was provided in the Supporting Information (Table S1). Cocrystal screening was conducted using the well-established solvent based and solid-state grinding techniques. Details of structural analysis, thermal, spectroscopic and physicochemical properties of the TG cocrystals are discussed in the following sections.

Table 1. CSD statistics on supramolecular synthons involving –CO–NH–CO– and some selected functional groups.

Moiety present together with –CO–NH–CO–	No. of structures	Supramolecular synthon	Occurrence of the synthon
	1822[a]	imide-imide (synthon I)	693 (38 %)
–OH	605	OH···carbonyl$_{imide}$ (synthon VI)	381 (63 %)
		synthon I and VI	82 (14 %)
H_2O	208	N–H$_{imide}$···O$_{water}$ (synthon V)	63 (30 %)
pyridyl	85	N–H$_{imide}$···N$_{pyridyl}$ (synthon IV)	45 (53 %)
–COOH	59	imide-acid (synthon II)	8 (14 %)
–CONH$_2$	15	N–H$_{amide}$···O$_{imide}$	13 (87 %)
		N–H$_{imide}$···O$_{amide}$	7 (47 %)
		amide-amide (synthon III)	3 (20 %)
		imide-amide (synthon VII)	2 (13 %)

[a] represents all the crystal structures that contain the –CO–NH–CO– moiety.

Crystal structures.

TG-NA (1:1) cocrystal. The cocrystal was prepared by crystallization from methanol. Alternatively, pure samples of the cocrystals were also prepared in bulk by solid-state grinding (see Supporting Information, Figures S1-S5). Crystal structure analysis revealed that the cocrystal belongs to triclinic, *P*-1 space group with one molecule each of TG and NA in the asymmetric unit (Table 2). In the crystal structure, two strong hydrogen bonds, N$_{amide}$–H···O$_{imide}$ (Table 3) hydrogen bond involving *syn*-N–H of the NA and O of one of the carbonyl of pyrimidinedione of the TG and N–H···N (synthon IV)

hydrogen bond involving N–H of the pyrimidinedione and pyridyl N of the NA, form a four-component supramolecular unit (Figure 3). The overall crystal structure is built up by columnar arrangement of four-component supramolecular units along the crystallographic *a*-axis via N–H_{anti}···O hydrogen bond involving the amide group of NA and π···π interactions. The hydrogen bonded columns are interconnected to each other via several C–H···O and C–H···F interactions.

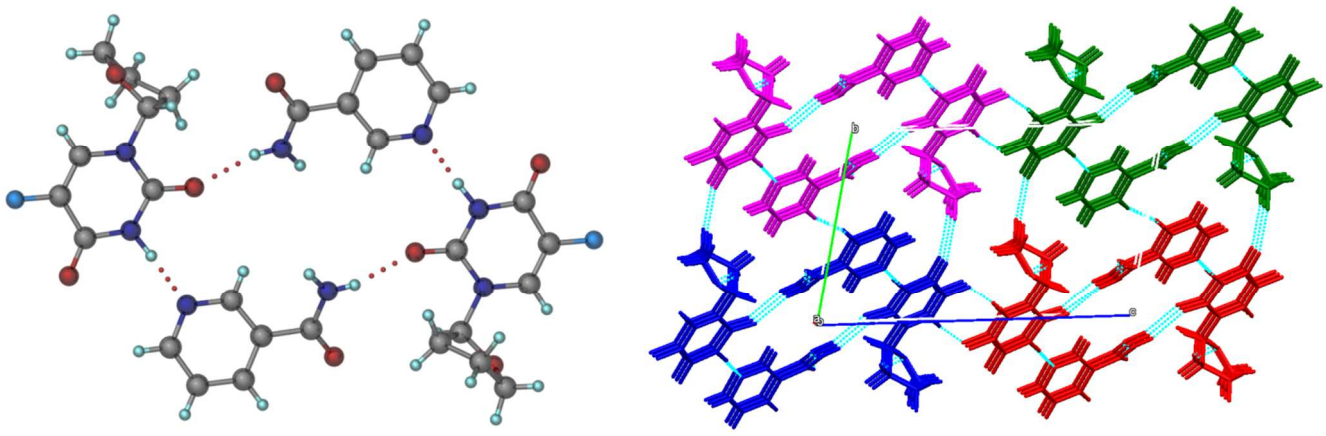

(a) **(b)**

Figure 3. Crystal structure of TG-NA cocrystal, (a) a four-component hydrogen bond supramolecular unit, (b) columnar arrangement of four-component supramolecular units via $N–H_{amide}···O_{amide}$ hydrogen bond (symmetry generated columns are shown in different colors).

TG-INA (1:1) cocrystal. Cocrystallization of TG and INA in 1:1 molar ratio from methanol gave a 1:1 cocrystal. The crystal structure was solved and refined in triclinic, *P*-1 space group with one molecule each of TG and INA. Similar to the crystal structure of TG-NA cocrystal, the TG-INA cocrystal also features a four-component supramolecular unit composing two molecules each of TG and INA, with the exception that the *anti*-N-H of the INA now forms $N_{amide}–H···O_{imide}$ hydrogen bond with the carbonyl O of the pyrimidinedione of TG (Figure 4). The amide group of INA forms an amide-amide homosynthon (synthon III) involving *syn*-N-H and carbonyl O. Thus, the crystal structure

is composed of infinitely hydrogen bonded four-component supramolecular units via the amide-amide homosynthon. These hydrogen bonded chains are interconnected in the crystal structure via several C–H···O, C–H···F, and π···π interactions.

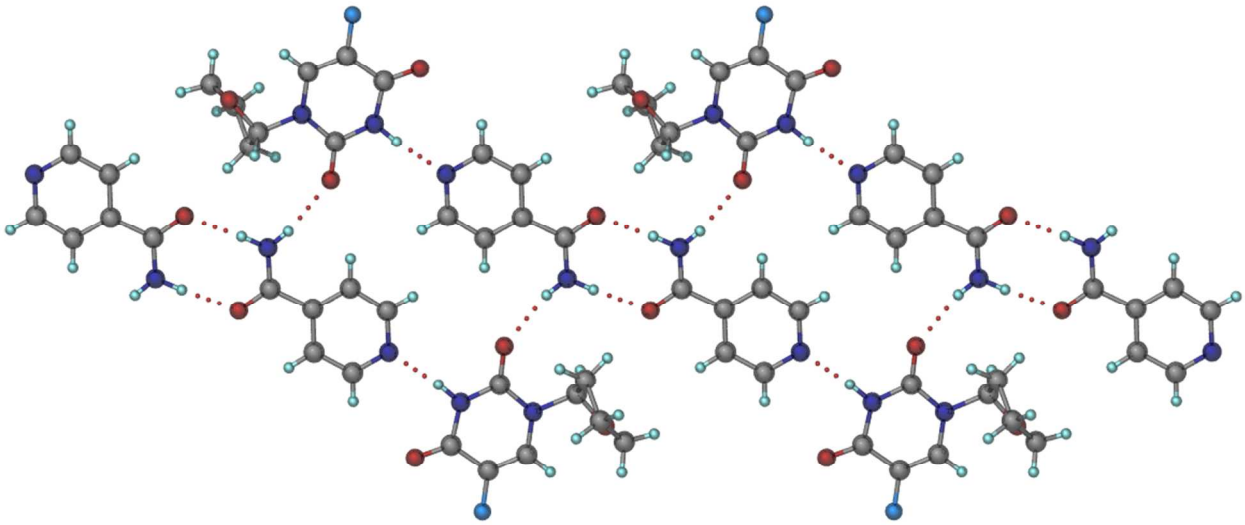

Figure 4. A part of the crystal structure of the TG-INA cocrystal. Notice the heterosynthon between TG and INA and homosynthon (synthon III) between INA molecules.

TG-4HBA (1:1) cocrystal. TG was found to form a 1:1 cocrystal with 4HBA when the cocrystallization was conducted in acetonitrile. Crystal structure of the TG-4HBA cocrystal belongs to monoclinic, $P2_1/n$ space group. Asymmetric unit contains one molecule each of TG and 4HBA. The crystal structure features a four-component supramolecular unit via heterosynthons, imide-acid (synthon II) and hydroxyl-carbonyl (synthon VI) (Figure 5). The four-component supramolecular units self-assemble in the crystal structure via several C–H···O, C–H···F, and π···π interactions.

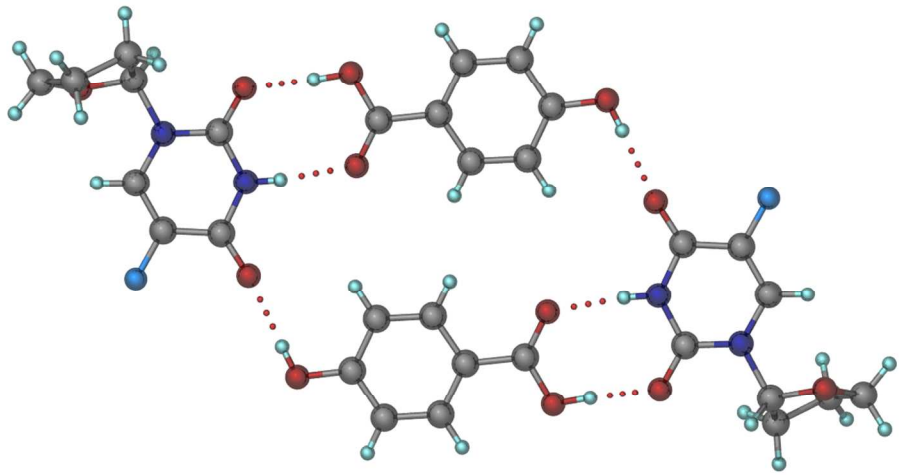

Figure 5. A four-component supramolecular unit in the crystal structure of TG-4HBA cocrystal.

TG-PG (1:1) cocrystal. A 1:1 cocrystal of TG and PG was identified when solvent evaporative cocrystallization was conducted in methanol. Crystal structure of the cocrystal belongs to monoclinic, *C*2/*c* space group with one molecule each of TG and PG in the asymmetric unit. PG can adopt five different conformations depending on the orientation of the hydroxyl groups.[39,40] All the hydroxyl groups of the conformer observed in the TG-PG cocrystal are on the same side which facilitate two cooperative intramolecular hydrogen bonds and has been found to be the stable conformer among the 5 possible conformers of PG.[39,40] The crystal structure of the TG-PG cocrystal is composed of a complex hydrogen bonded network due to the presence of multiple hydrogen bond donors and acceptors (Figure 6). However, the crystal structure could be better understood in terms of dimers of TG and PG molecules mediated by imide-imide (synthon I) and hydroxyl-hydroxyl homosynthons, respectively, which are interconnected via hydroxyl-carbonyl heterosynthon (synthon VI). The resulting two dimensional sheets are further self-assemble via O–H···O hydrogen bonds, and C–H···O and C–H···F interactions.

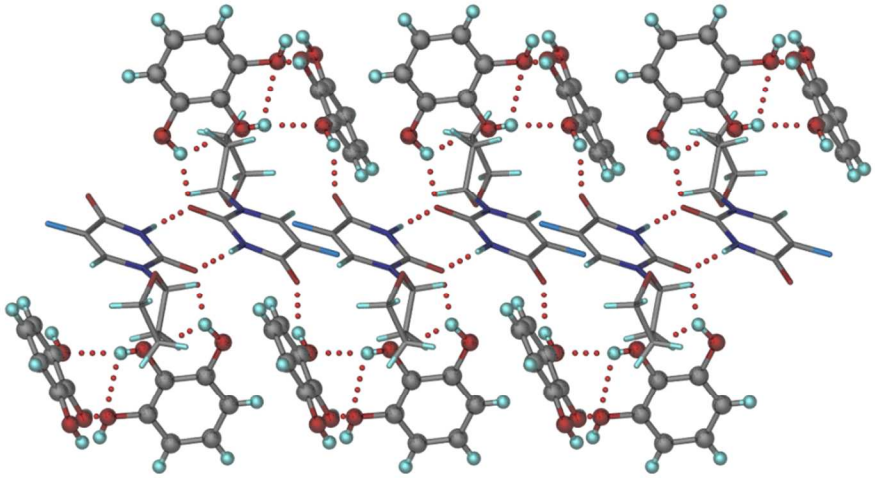

Figure 6. A part of the crystal structure of TG-PG cocrystal. Notice the dimers of TG and PG molecules mediated by homosynthons. TG molecules are shown in stick model and PG molecules are shown in ball and stick model.

TG-TP (1:1) cocrystal monohydrate. TP is a central nervous system stimulant which is also used for the treatment of respiratory diseases such as asthma.[41] Solvent evaporative cocrystallization of a 1:1 molar ratio of TG and TP from acetonitrile provided crystals that were confirmed by crystal structure analysis as TG-TP (1:1) cocrystal monohydrate. Crystals of the TG-TP cocrystal hydrate belong to triclinic *P*-1 space group and the asymmetric unit contains one molecule each of TG, TP, and water. Serendipitous discovery of cocrystal hydrates from attempted cocrystallization experiments is not uncommon, and several such cases have been reported recently.[42-46] The unintended inclusion of water as an integral part of the cocrystal renders cocrystal design strategies and has recently been referred to as nemesis of crystal engineering.[43] The imidazole N's and carbonyl groups of TP are known to form a variety of intermolecular interactions in the cocrystals, such as carboxyl···$N_{imidazole}$, hydroxyl···$N_{imidazole}$, hydroxyl···$O{=}C_{urea}$, hydroxyl···$O{=}C_{amide}$, $N{-}H_{imidazole}$···$O{=}C_{urea}$, $N{-}H_{amide}$···$O{=}C_{amide}$, etc.[47-49] A CSD survey of the crystal structures that contain –CO–NH–CO– and

imidazole moieties resulted in 19 crystal structures, of which in 8 (42 %) crystal structures the N-H of the –CO–NH–CO– moiety forms N–H···N hydrogen bond with the N of the imidazole.[38] Therefore, it is expected that a cocrystal involving TG and TP may also features the same interaction. However, the presence of water molecule in the crystal lattice results in competition among the various intermolecular interactions and the N–H of TG forms N–H···O hydrogen bond (synthon V) with the water molecule (Figure 7). The water molecule forms two additional O–H···O hydrogen bonds with $O{=}C_{amide}$ and imidazole N of the TP. This results in a hydrogen bonded chain which also features N–H···O hydrogen bond involving imidazole N–H of TP and $O{=}C_{urea}$ of TG. Symmetry related hydrogen bonded chains in the crystal structure are connected to each other via several C–H···O and C–H···F interactions.

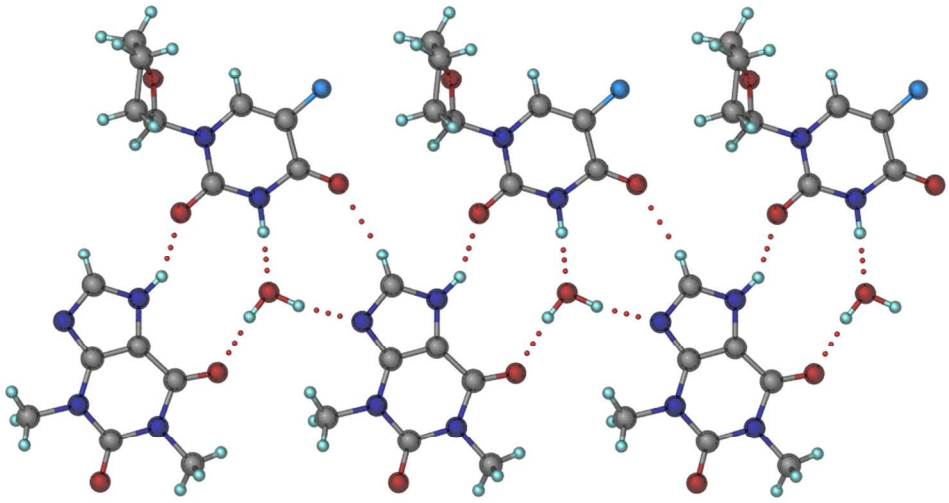

Figure 7. A part of the crystal structure of the TG-TP cocrystal hydrate.

The observed supramolecular synthons in the TG cocrystals are in line with the CSD statistics. For example, in the case of coformers that contain amide and pyridyl groups (NA and INA), the N–H of the –CO–NH–CO– moiety of TG preferentially forms N–H···N hydrogen bond (synthon IV) with the

pyridyl N. In addition, both the cocrystals feature N–H_{amide}···O_{imide} hydrogen bond, which is the most abundant synthon in the crystal structures that contain amide and –CO–NH–CO– moieties. The absence of a two-point imide-amide synthon (synthon VII) in these crystal structures could be reasoned to the formation of (a) an infinite hydrogen bond chain of NA molecules involving the amide group via N–H···O hydrogen bond in the TG-NA cocrystal, (b) an amide-amide homosynthon in the TG-INA cocrystal, which form extended hydrogen bond networks and further stabilize the crystal structures. Both the cocrystals that contain phenolic coformers (4HBA and PG) feature O–H···O hydrogen bond (synthon VI), in addition, while the cocrystal with 4HBA features acid-imide synthon (synthon II), the cocrystal with PG features imide-imide homosynthon (synthon I). In the case of the cocrystal hydrate (with TP), although the N-H of the –CO–NH–CO– moiety is expected to form N–H···N hydrogen bond with the N of the imidazole, it forms N–H···O hydrogen bond (synthon V) with the O of the water molecule which is in agreement with the previous precedents in the literature concerning the crystalline hydrates that feature –CO–NH–CO– moiety. Overall, the persistence of supramolecular synthons in TG cocrystals in line with the CSD statistics attests the greater role of supramolecular synthon approach in the successful cocrystal design.

Spectroscopic Analysis of Cocrystals.

Cocrystal formation often results in conformational and structural variations of the constituent components that can be determined by spectroscopic techniques. For example, Fourier transform Infrared (FT-IR) spectroscopy is used for measuring vibrational modes of a compound, and therefore, the technique is effective in detecting the changes in vibrational modes of the functional groups responsible for the cocrystal formation.[50] As evident from the crystal structures of the cocrystals

(Figures 3-7), the carbonyl and N–H groups of the pyrimidinedione ring are the main functional groups involved in cocrystal formation, and hence changes in vibrational modes of these functional groups are considered for identification of cocrystal formation. Commercial sample of TG used in the present study belongs to α-polymorph (CSD Refcode: BIPDEJ01) based on comparison of the powder X-ray diffraction (PXRD) patterns (see Supporting Information, Figure S6).[28] Crystal structure of the α-form has two conformationally different symmetry independent molecules. The carbonyl groups on the pyrimidinedione ring showed three absorption bands consistent with the previous observation at 1655 cm^{-1} and 1689 cm^{-1} for the hydrogen bonded carbonyl group and at 1718 cm^{-1} for the free carbonyl group (Table 4, Figure 8).[31] The N–H stretching in TG was observed as a broad peak at 3426 cm^{-1}. Changes in vibrational modes are evident from the cocrystal formation. For example, the N–H group of TG is involved in N–H···O hydrogen bond with itself in the α-form and in TG-PG cocrystals and hence the N–H and C=O stretching vibrations were observed at approximately the same wave length in both the solids. In the case of the cocrystals, TG-NA, TG-INA, and TG-4HBA, the N–H group of TG is involved in N–H···O or N–H···N hydrogen bond with the coformer molecule, therefore the difference in hydrogen bond compared to the parent α-form is reflected as bathochromic shift in all the cocrystals. In the case of the TG-TP cocrystal hydrate, the N–H of TG is involved in N–H···O hydrogen bond with the water molecule, which results in a significant hypsochromic shift in the stretching mode. Similarly, the free carbonyl group of TG which is not involved in strong hydrogen bond in α-form is involved in strong O–H···O hydrogen bond in TG-4HBA and TG-PG cocrystals, and involved in multiple C–H···O interactions in the other cocrystals, therefore, resulting in changes in the C=O stretching vibration from 1718 cm^{-1} in the α-form to 1693-1705 cm^{-1} in the cocrystals. All the observed variations in the vibrational modes were consistently observed in multiple measurements of FT-IR spectra.

Table 4. Vibration frequencies of the selected bonds partaking in hydrogen bonding

Vibration Frequency (cm^{-1})	TG	TG-NA	TG-INA	TG-4HBA	TG-TP hydrate	TG-PG
C4=O2	1655, 1689	1668, 1692	1653, 1681	1654, 1686	1651, 1695	1647, 1683
C1=O1	1718	1705	1701	1703	1693	1714
N1–H	3418	3412	3406	3376	3433	3412

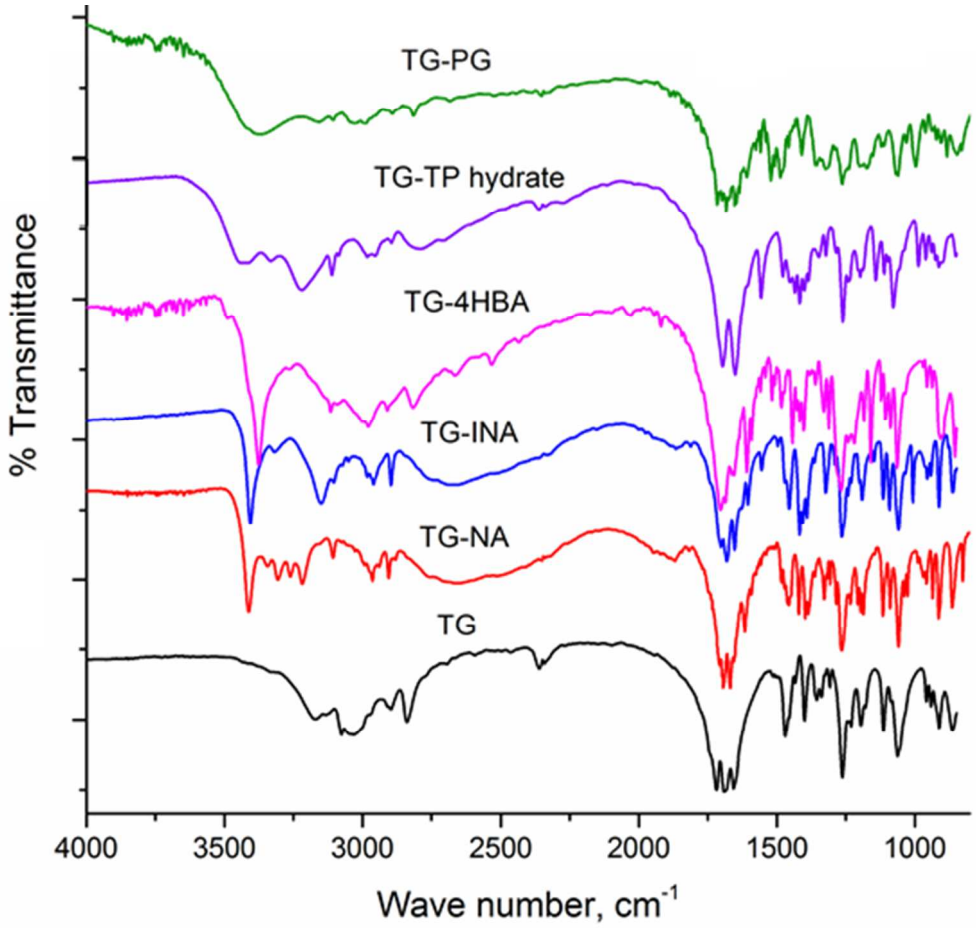

Figure 8. Comparison of the FT-IR spectra of TG and its cocrystals.

Thermal analysis

All the cocrystals reported in this paper were analyzed by differential scanning calorimetry (DSC) and thermogravimetric analysis (TGA). The thermal data provided an accurate melting point and decomposition of the solids analyzed (Table 5). Thermal behavior of TG (α-form) is consistent with the previous observation that showed two endothermic peaks at 165 °C and 172 °C (Figure 9).[31] The first endothermic peak is attributed to the polymorphic transformation from the α-form to the γ-form and the second peak is due melting of the γ-form. Melting point of all the cocrystals is lower than the melting point of the cocrystal constituents. In addition to the melting endotherm at 120 °C, TG-PG cocrystal shows a post melting crystallization exotherm at 170 °C. In the case of TG-TP cocrystal hydrate, water loss from the crystal lattice was observed between 100 and 115 °C. The remaining solid after the water loss melts at 155 °C.

Table 5. Thermophysical data for the cocrystals and literature melting point data of the coformers.

	Melting point of the coformer (°C)	Melting point of the cocrystal (°C)	ΔH (J g^{-1})
TG	171.7		101.2
TG-NA	128	105.2	136.2
TG-PG	131-134	120	134.8 (melting)
TG-INA	155-157	149.4	164.7
TG-4HBA	214.5	139.7	210.4
TG-TP hydrate	273	101.9 (dehydration)	58.3 (dehydration)
		155.5	58.9 (melting)

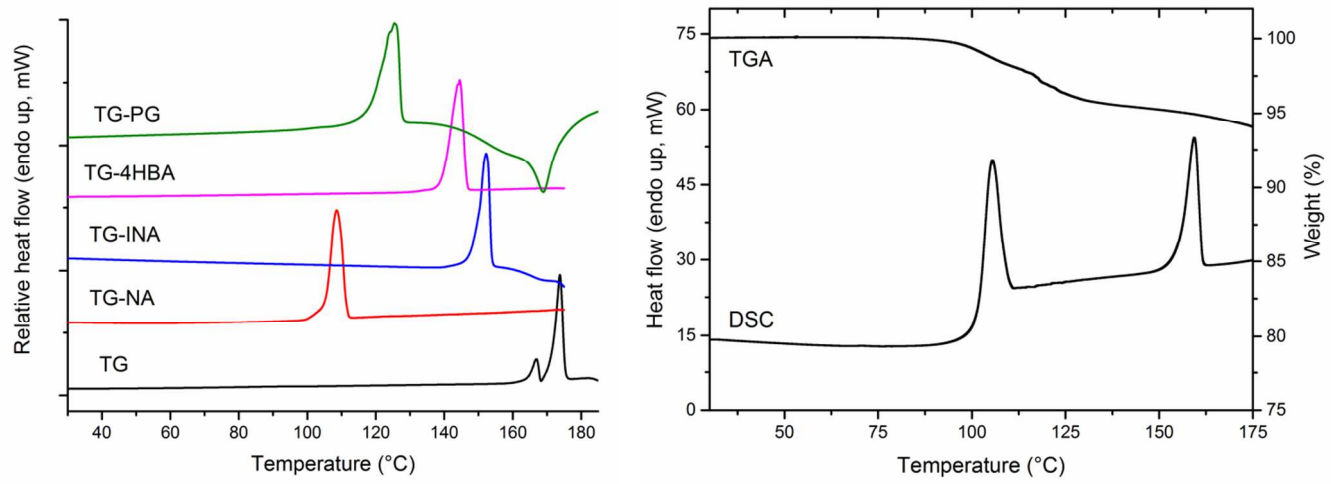

(a) **(b)**

Figure 9. Thermograms of the solids reported in this paper, (a) DSC profiles of the anhydrous cocrystals, (b) TGA and DSC profile of the TG-TP cocrystal hydrate.

Stability of the cocrystals

A combination of temperature and humidity is necessary to evaluate the stability of a drug substance or drug product. The International Conference on Harmonisation (ICH) guidelines provide stability testing protocols for regulatory submission, covering storage, intermediate, accelerated and stress conditions.[51] Stability studies are generally conducted at accelerated storage condition, wherein the samples are stored at 40 °C and 75 % RH for 6 months. When a significant change occurs at the accelerated storage condition, additional testing at intermediate storage conditions should be conducted from 6 months to 12 months. In the present study, all the TG cocrystals were stored at accelerated test condition for 13 weeks and stability of the cocrystals was assessed by comparing the PXRD pattern of the samples measured at regular intervals. Stability results revealed that all the cocrystals remain the same and do not undergo dissociation or degradation (see Supporting Information Figure S7-S11).

Stability of the cocrystals was also tested by performing slurry experiments at 37 °C and using the DVS technique. In slurry experiments, excess powder samples of the cocrystals were stirred in pH 6.8 buffer at 37 °C for 24 h. Filtered and air-dried samples were analyzed by PXRD for their identity. The stability experiments revealed that the TG-INA, TG-TP hydrate, and TG-4HBA cocrystals were stable under slurry conditions (Figure 10). Neither dissociation of the cocrystal nor chemical degradation of the cocrystal constituents was observed. In the case of TG-NA and TG-PG cocrystals, the solids remained after the slurry experiment matched with β- and α-polymorphs of the TG, respectively. This suggests that the cocrystals dissociated under slurry conditions; the highly soluble NA and PG dissolved into the solution and the poorly soluble TG remained as the solid. Interestingly, the dissociation of the cocrystals to its constituents led to selective formation of the β-polymorph of TG in the case TG-NA cocrystal, and α-polymorph in the case of TG-PG cocrystal. Under identical slurry conditions the α-polymorph remained the same. Therefore, the TG-NA and TG-PG cocrystals offer an alternative route to selective preparation of the pure α and β-polymorphs of TG.

The DVS technique measures moisture uptake by a sample at constant temperature. The DVS profiles in Figure 11 revealed that all the cocrystals and TG show negligible moisture uptake (< 1 %) suggesting that the cocrystals and TG are stable at even at high RH conditions. TP is hygroscopic and is known to interconvert between crystalline anhydrate and monohydrate forms as a function of RH.[52] Therefore, as shown in Figure 11, TP shows significant moisture uptake (9.2 %) during the sorption profile which very well agrees with the weight gain expected for the monohydrate (9.1 %) formation.

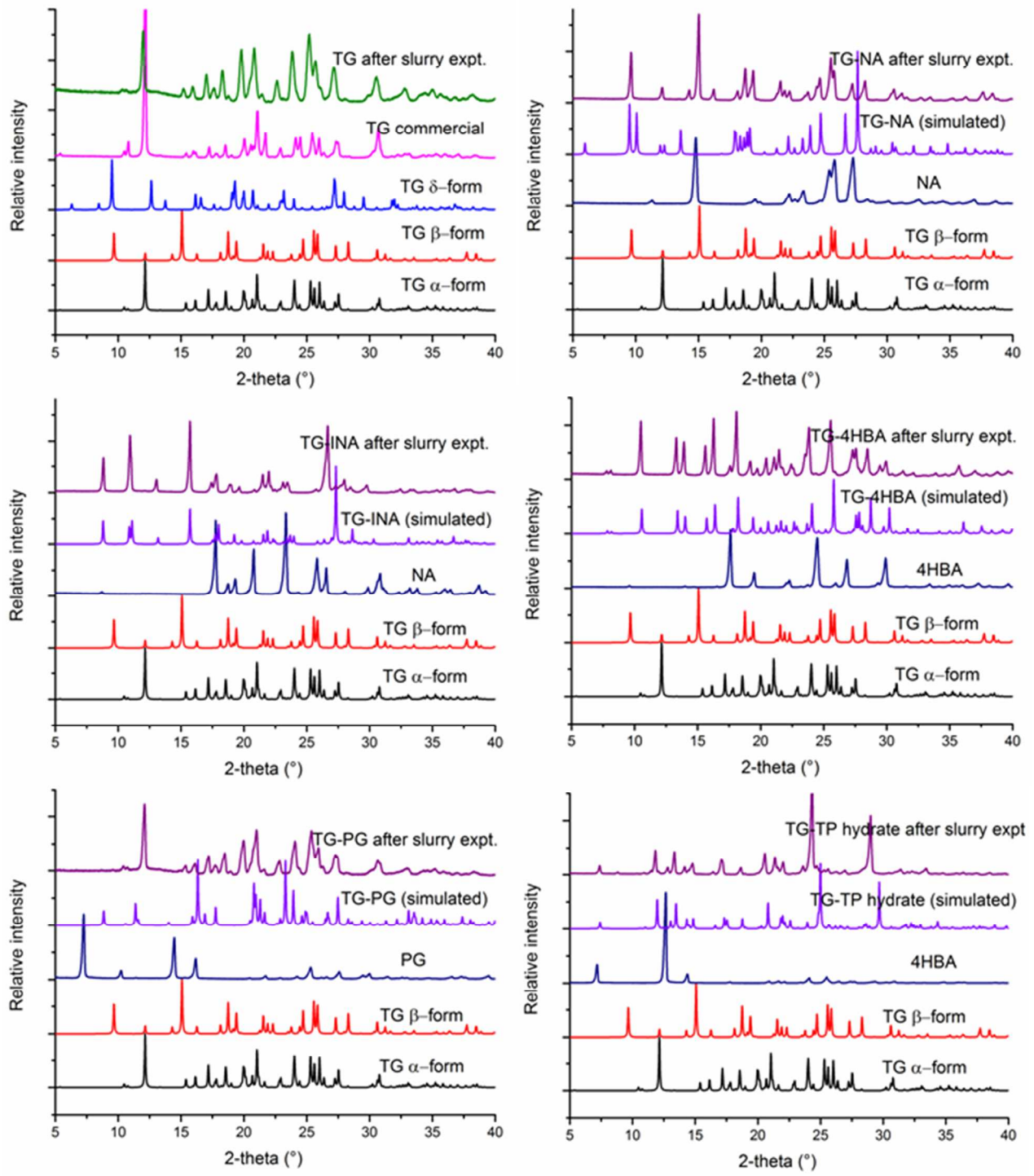

Figure 10. Overlay of PXRD patterns of the samples from slurry stability test. Notice that while TG-NA and TG-PG cocrystals dissociate and convert to β-form and α-form of TG, respectively, all other cocrystals and TG are stable under slurry conditions.

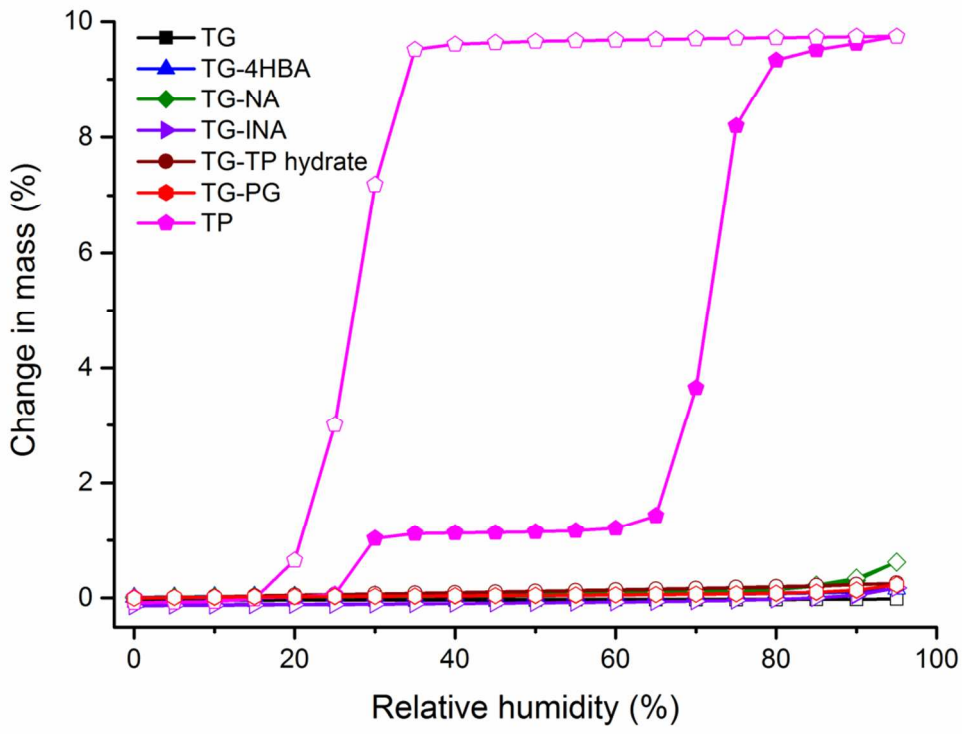

Figure 11. DVS sorption/desorption profiles of TG, TP, and the cocrystals. Profiles designated with solid and open legends correspond to sorption and desorption profiles, respectively.

Solubility and intrinsic dissolution rate (IDR).

Equilibrium concentration (thermodynamic solubility) and maximum concentration (kinetic solubility) are critical in predicting and optimizing a drug performance. Therefore, determining the solubility is an essential step in assessing the developability of a drug. Solubility and dissolution rate of the TG, TP, and cocrystals were measured in pH 6.8 phosphate buffer at 37 °C. Excess solids of the TG, TP, and the cocrystals were slurried in pH 6.8 buffer and after equilibration, filtered solids were analyzed by PXRD and concentration of the aliquots was quantified by high-performance liquid chromatography (HPLC). The results of the slurry stability tests in Figure 10 revealed that the TG-NA

cocrystal converted to β-polymorph of the TG, and TG-PG cocrystal converted to the α-polymorph of the TG. Therefore, in these cases, calculation of apparent dissolution rate constant provides a good representation of the solubility of the cocrystals.[53,54] The apparent solubility of the unstable cocrystals was calculated according to the literature procedure.[53,54] PXRD pattern of the remaining solids from the slurry experiments of the other cocrystals complies well with the corresponding cocrystals and hence the measured solubility is the true solubility of the respective cocrystals. The solubility values are listed in Table 6. The TG-INA cocrystal showed the highest solubility, which is ~2.3 times the solubility of the TG. Similarly TG-NA and TG-PG cocrystals also showed slight improvement in the solubility of TG. In case of the other cocrystals, solubility values are lower than the solubility of the parent TG. In the case of TG-TP cocrystal hydrate, solubility of TG decreased but solubility of TP improved. The observed solubility of the TG and cocrystals follows the trend: TG-INA > TG-NA > TG-PG > TG > TG-4HBA > TG-TP cocrystal hydrate.

Intrinsic dissolution rate (IDR) is defined as the dissolution rate of a substance, where the conditions of surface area, temperature, agitation, and medium pH and ionic strength are all constant.[55] Figure 12 shows the IDR profiles of the TG, TP and cocrystals and the calculated IDR values are tabulated in Table 6. Analysis of the samples after the dissolution experiments by PXRD confirmed that the solids remained the same, suggesting that there was no dissociation of the cocrystals (see Supporting Information Figures S12-S16). Comparison of the calculated IDR values suggests that the dissolution rate follows the observed solubility trend and suggests that the TG-INA cocrystal is the fastest dissolving cocrystal among all the cocrystals in this study. The IDR follows the trend: TG-INA > TG-NA > TG-PG > TG > TG-4HBA > TG-TP hydrate. The solubility and dissolution rate measurements confirm that TG-INA cocrystal is stable under slurry conditions and showed improved solubility and dissolution rate and hence INA is the most promising coformer for developing TG formulations.

Table 6. Equilibrium solubility and IDR values of TG, TP and cocrystals reported in this paper.

Solid form	Equilibrium solubility (mg ml^{-1})	Apparent solubility (mg ml^{-1})	IDR ($\times 10^{-2}$) (mg cm^{-2} min^{-1})
TG	23.3		3.5
TP	7.4		1.4
TG-TP hydrate (TG)	16.1 (× 0.7)		1.8 (× 0.5)
TG-TP hydrate (TP)	13.7 (× 1.9)		1.6 (× 1.1)
TG-4HBA	16.8 (× 0.7)		2.0 (× 0.6)
TG-NA	-	30.0 (× 1.3)	4.5 (× 1.3)
TG-INA	53.9 (× 2.3)		5.5 (× 1.6)
TG-PG	-	28.6 (× 1.2)	4.3 (× 1.2)

Values in the parenthesis indicate the extent of increment in solubility and dissolution rate with respect to TG or TP.

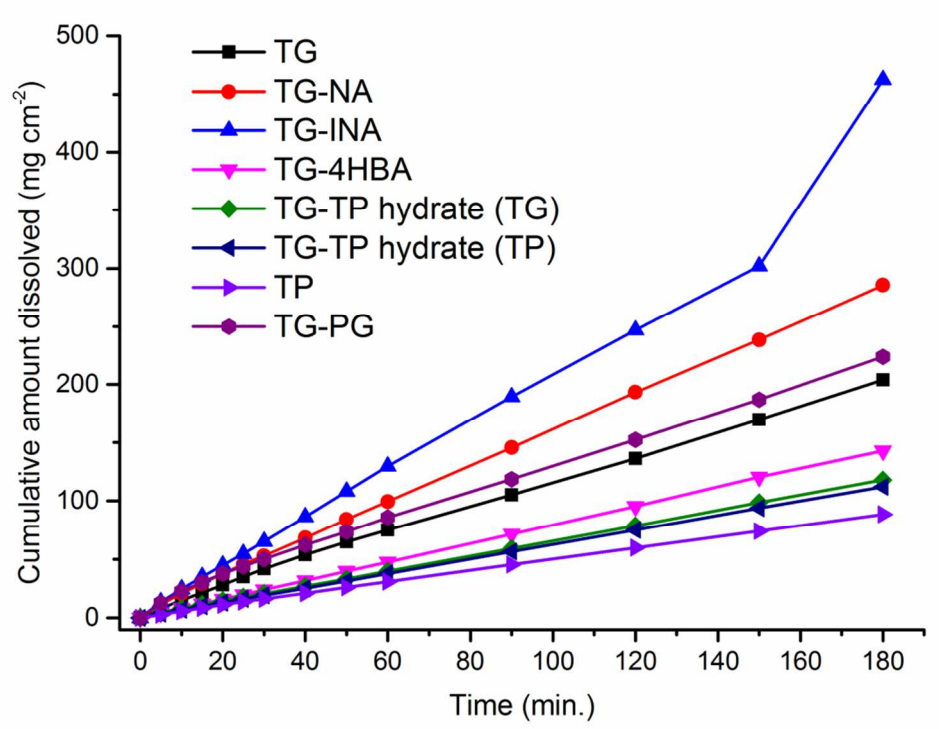

Figure 12. IDR profiles of TG, TP, and the cocrystals reported in this paper.

CONCLUSIONS

We have prepared five cocrystals of a chemotherapy agent, TG, with pharmaceutically acceptable coformers. The design of cocrystals was made possible by the statistical analysis of the hydrogen bonding capability of the functional group present on the TG molecule. Crystal structure analysis revealed the formation of cocrystals based on the hydrogen bonds prevalent in the family of crystal structures retrieved from the Cambridge Structural Database. Imide-imide homosynthon is the most common intermolecular interaction in the TG polymorphs. A crystal engineering approach was utilized to identify the suitable coformers that could preferentially form heterosynthons with the TG; as such 4 of the 5 crystal structures reported herein feature the expected heterosynthons. All the new solids were characterized by FT-IR, thermal analysis and X-ray diffraction techniques. Stability of the cocrystals was tested by storage at accelerated test condition (40 °C, 75 % RH), slurry and dynamic vapor sorption experiments. All the cocrystals were found to be stable at accelerated test condition. Slurry experiments revealed that the TG-NA and PG-PG cocrystals dissociated and converted to β-and α-polymorph of the TG, respectively. TG-INA, TG-4HBA, and TG-TP hydrate were found to be stable under the slurry conditions. Solubility and dissolution experiments in pH 6.8 phosphate buffer confirmed the higher solubility and dissolution rate of the cocrystals with INA, NA and PG. Based on the experimental data presented herein, the TG-INA cocrystal is the promising cocrystal for development of TG formulations. The cocrystal is stable under various stability conditions and improves the solubility/dissolution rate of TG.

EXPERIMENTAL SECTION

All the chemicals used in this study were purchased from commercial sources: TG (> 98 % purity)-Tokyo Chemical Industry Co. Ltd, Singapore, TP-anhydrous (99 %) – Sigma-Aldrich, NA (99 %) – Fluka-Sigma Aldrich, INA (99 %) – Alfa Aesar, 4HBA (99 %) – Alfa Aesar, and PG (>98 %) – Sigma-Aldrich. Analytical grade solvents were used for the crystallization experiments.

Solvent Based Cocrystallization. Crystalline cocrystal samples were prepared by solvent-evaporative crystallization under ambient conditions.

TG-NA cocrystal. TG (200.2 mg, 1 mmol) and NA (122.1 mg, 1 mmol) were dissolved in 10 mL of methanol at 60 °C and left for evaporation of the solvent at ambient conditions. Single crystals of the TG-NA (1:1) cocrystal were obtained as colorless blocks after 5 days.

TG-INA cocrystal. TG (200.2 mg, 1 mmol) and INA (122.1 mg, 1 mmol) were dissolved in 10 mL of methanol at 60 °C and left for evaporation of the solvent at ambient conditions. Single crystals of the TG-INA (1:1) cocrystal were obtained as colorless needles in 5 days.

TG-4HBA cocrystal. TG (200.2 mg, 1 mmol) and 4HBA (136.2 mg, 1 mmol) were dissolved in 10 mL of acetonitrile at 70 °C and left for evaporation of the solvent at ambient conditions. Single crystals of the TG-4HBA (1:1) cocrystal were obtained as colorless needle in 3 days.

TG-PG cocrystal. TG (200.2 mg, 1 mmol) and PG (126.1 mg, 1 mmol) were ground using ball-mill for 30 min at a frequency of 20 Hz and the resulting powder was dissolved in 10 mL of methanol at 50 °C and left for evaporation of the solvent at ambient conditions. Single crystals of the TG-PG (1:1) cocrystal were obtained as colorless needles in 10 days.

TG-TP cocrystal hydrate. TG (200.2 mg, 1 mmol) and TP (180.2 mg, 1 mmol) were dissolved in 10 mL of acetonitrile at 75 °C and left for evaporation of the solvent at ambient conditions. Single crystals of the TG-TP cocrystal hydrate (1:1:1) were obtained as colorless needles in 5 days.

Grinding Experiments. Grinding was performed using a Retsch Mixer Mill model MM301 with 10 mL stainless steel grinding jars with one 7 mm stainless steel grinding ball at a rate of 20 Hz for 30 min. Experiments were carried out with 200.2 mg (1 mmol) of TG and the corresponding amount of coformer. SDG experiments were conducted with 2 drops of methanol prior to grinding.

Single Crystal X-ray Diffraction. A good quality single crystal grown from solution crystallization was chosen under a Leica microscope and placed on a fibre needle which was then mounted on to the goniometer of the X-ray diffractometer. X-ray reflections were collected on a Rigaku Saturn CCD area detector with graphite monochromated Mo-Kα radiation (λ = 0.71073 Å). Data were collected and processed using CrystalClear (Rigaku) software. Structure was solved by direct methods and SHELX-TL[56] was used for structure solution and least-squares refinement. The non-hydrogen atoms were refined anisotropically. H atoms bonded to N and O atoms were located in the difference electron density map and allowed to ride on their parent atoms in the refinement cycles. All other H atoms were positioned geometrically and refined using a riding model. All O–H, N–H and C–H distances are neutron normalized to 0.983, 1.009 and 1.083 Å, respectively. X-Seed[57] was used to prepare the packing diagrams. CCDC 1023620-1023624 contains the supplementary crystallographic data for this paper. These data can be obtained free of charge from The Cambridge Crystallographic Data Centre via http://www.ccdc.cam.ac.uk/conts /retrieving.html and deposited as Supporting Information.

Powder X-ray Diffraction (PXRD). The powder materials were identified by D8 Advance powder X-ray diffractometer (Bruker AXS GmbH, Germany) with Cu-Kα radiation (λ = 1.54056 Å). The

voltage and current applied were 35 kV and 40 mA, respectively. Samples were placed on the sample holder which has 1 mm thickness and 1.5 cm diameter. The sample was scanned within the scan range of 2θ = 5° to 50° continuous scan, with a scan rate of 2 deg min^{-1}. The PXRD patterns were plotted using OriginPro 7.5.

Thermal Analysis. DSC was performed with a Perkin Elmer Diamond DSC with an Autosampler. Crystals taken from the mother liquor were blotted dry with a filter paper and manually ground. The samples were placed in crimped but vented aluminum sample pans. The sample size was 5-10 mg and the heating rate was 10 °C min^{-1}. The samples were purged with a stream of flowing nitrogen (20 mL min^{-1}). The instrument was calibrated using indium as the reference material.

TGA was performed on a TA instruments TGA Q500 thermogravimetric analyzer. Approximately 15 mg of the sample was added to an alumina crucible. The samples were heated over the temperature range of 25 to 300 °C at a constant heating rate of 10 °C min^{-1}. The samples were purged with a stream of flowing nitrogen throughout the experiment at 40 mL min^{-1}.

Relative humidity (RH) stability studies. Stability of all the cocrystals was tested at 40 °C, 75 % RH condition. Approximately 150 mg of each of the cocrystals was placed in petri dish and stored in ESPEC SH-241 Bench-top temperature & humidity chamber. The temperature and RH of the stability chamber were maintained at 40 °C and 75 %, respectively, throughout the test period. The stored samples were analyzed at regular intervals by PXRD.

DVS measurements. Surface Measurement Systems Advantage Dynamic Vapour Sorption (DVS) instrument was used to determine the water vapour sorption isotherm. The uptake and loss of vapour were measured gravimetrically using a Cahn D200 recording ultra-microbalance with a mass resolution of ±0.1μm. Approximately 40 mg of all samples were used during each experiment. All

samples were initially dried for 180 min at 45 °C and 0 % partial vapor pressure. The relative humidity was than increased from 0 % to 95 % in 9 steps of around 10 % each and back to 0 % in a similar manner via desorption. The system was considered to be in equilibrium if the rate change of mass was less than 0.002 %/min at one specific partial vapour pressure. The temperature was maintained at a constant 25°C. The sorption isotherms were calculated from the equilibrium mass values.

Solubility and Dissolution Experiments. Solubility and dissolution experiments were performed in pH 6.8 phosphate buffer. TG and TP concentration from the solutions obtained in solubility and dissolution experiments were measured by HPLC (Agilent 1100 series). Individual methods were developed to make sure that the cocrystal components were observed at different retention times. In all the experiments, the HPLC instrument was equipped with a ZORBAX Eclipse XDB-C18 column (4.6 × 250 mm, 8 nm pore size, 5 μm). An injection volume of 10 μL was used at an eluent flow rate of 1 mL min^{-1}. Detection wavelength in the UV–visible range was set at 271 nm for TG and at 272 nm for TP. For the samples containing TP, the samples were eluted with a mobile phase containing a mixture of methanol and ultrapure water in a ratio (v/v) of 20:80. Using this method, the observed retention times are: TG - 6.27 min and TP - 7.41 min. For the cocrystal samples that do not contain TP, the samples were eluted with a mobile phase containing a mixture of ultrapure water, acetonitrile and water in a ratio (v/v) of 85:5:10. The observed retention times are as follows: TG – 7.64, NA – 3.77, INA – 3.63, and 4HBA – 2.56 min. Prior to the solubility and dissolution experiments, individual calibration plots for TG, TP, and cocrystals were constructed at a concentration range of 7–50 μg mL^{-1} and with R^2 of 0.99 (n = 3). The calibration plots for all the cocrystals were constructed based on the concentration of the TG calculated from molar ratio of the TG and coformer. For the cocrystals that were found unstable in solubility experiments, apparent solubility was calculated based on eq 1.

$$C_m = C_s(J_m/J_s) \quad (1)$$

where C_m is the apparent solubility of the cocrystal, C_s is the solubility of the thermodynamic form, and J_m and J_s are the dissolution rates of the cocrystal and the stable species.[24]

Equilibrium solubility values were determined using the shake-flask method by stirring an excess amount of each sample in 5 mL of the pH 6.8 buffer at 37 °C for 24 h. The solutions were filtered through 0.4 μm syringe filters, and the concentration of the solutions was determined using HPLC. IDR experiments were conducted using a Varian VK7010 dissolution apparatus equipped with a VK750D heater/circulator. In each experiment, approximately 500 mg of the sample was compressed to a 0.5 cm^2 disk in a USP-certified Electrolab rotating disk intrinsic dissolution die using a hydraulic press at a pressure of 5 tons for 5 min. Only one side of the disk was exposed to the dissolution medium and the surface of the disk was constant throughout the experiment. The intrinsic attachment was placed in a jar with 900 mL of phosphate buffer (pH 6.8) preheated at 37 °C and stirred at 50 rpm. At regular time intervals, 2 mL of the samples were withdrawn manually. The collected samples were filtered through 0.4 μm nylon filters and assayed for TG and TP concentrations using HPLC from the respective calibration plots.

Cambridge Structural Database (CSD) Analysis. Crystal structures that contain the –CO–NH–CO– moiety were retrieved from the CSD (using ConQuest Version 1.16, February 2014 update) using the following search filters: 3D coordinates determined, only organics, R-factor ≤ 0.1, not disordered, no errors, not polymeric, no ions, no powder structures. The search resulted in 1822 entries containing the –CO–NH–CO– moiety. Subsequent searches were conducted to identify the specific supramolecular interactions within the subset of 1822 entries.

ASSOCIATED CONTENT

Supporting Information. List of coformers used for cocrystal screening, PXRD plots of the samples obtained in grinding and dissolution experiments, TGA profiles of anhydrous cocrystals, and ORTEP plots of the crystal structures. This material is available free of charge via the Internet at http://pubs.acs.org/.

AUTHOR INFORMATION

Corresponding Authors

* (S.A.) E-mail: srinivasulu_aitipamula@ices.a-star.edu.sg

* (R.B.H.T) E-mail: reginald_tan@ices.a-star.edu.sg

Notes

The authors declare no competing financial interest.

ACKNOWLEDGMENT

We greatly acknowledge Science and Engineering Research Council of A*STAR (Agency for Science, Technology and Research) for providing financial support. We also thank Ms. Annie B. H. Wong and Mr. Khoo Yi Hao for technical assistance.

REFERENCES

(1) Aitipamula, S.; Nangia, A. *Polymorphism: Fundamentals and Applications. In Supramolecular Chemistry: From Molecules to Nanomaterials*; Steed, J. W., Gale, P. A., Eds.; John-Wiley: New York, **2012**; pp 2957–2974.

(2) Desiraju, G. R. *J. Am. Chem. Soc*., **2013**, *135*, 9952–9967.

(3) Desiraju, G. R.; Vittal, J. V.; Ramanan, A. *Crystal Engineering: A Textbook*, 1st ed.; World Scientific Publishing Company Incorporated: New Delhi, **2011**; pp 77–95.

(4) Aakeröy, C. B.; Champness, N. R.; Janiak, C. *CrystEngComm,* **2010**, *12*, 22-43.

(5) Jones, W.; Motherwell, W. D. S.; Trask, A. V. *MRS Bull.* **2006**, *31*, 875-879.

(6) Almarsson, Ö.; Zaworotko, M. J. *Chem. Commun.* **2004**, 1889-1896.

(7) Walsh, R. D. B.; Bradner, M. W.; Fleischman, S. G.; Morales, L. A.; Moulton, B.; Rodríguez-Hornedo, N.; Zaworotko, M. J. *Chem. Commun.* **2003**, 186-187.

(8) Yan, D.; Delori, A.; Lloyd, G. O.; Friščić, T.; Day, G. M.; Jones, W.; Lu, J.; Wei, M.; Evans, D. J.; Duan, X. *Angew. Chem. Int. Ed.* **2011**, *50*, 12483-12486.

(9) Karki, S.; Friščić, T.; Fábián, L.; Laity, P. R.; Day. G. M.; Jones, W. *Adv. Mat.* **2009**, *21*, 3905-3909.

(10) Aitipamula, S.; Vangala, V. R.; Chow, P. S.; Tan, R. B. H. *Cryst. Growth Des.* **2012**, *12*, 5858–5863.

(11) Cherukuvada, S.; Babu, N. J.; Nangia, A. *J. Pharm. Sci.* **2011**, *100*, 3233–3244.

(12) Babu, N. J.; Sanphui, P.; Nangia, A. *Chem. Asian J.* **2012**, *7*, 2274-2285; (d) Suresh, K.; Goud, N. R.; Nangia, A.; *Chem. Asian J.* **2013**, *8*, 3032-3041.

(13) Hickey, M. B.; Peterson, M. L.; Scoppettuolo, L. A.; Morrisette, S. L.; Vetter, A.; Guzmán, H.; Remenar, J. F.; Zhang, Z.; Tawa, M. D.; Haley, S.; Zaworotko, M. J.; Almarsson, Ö. *Eur. J. Pharm. Biopharm.* **2007**, *67*, 112–119.

(14) Childs, S. L.; Kandi, P.; Lingireddy, S. R. *Mol. Pharmaceutics,* **2013**, *10*, 3112-3127.

(15) Chadha, R.; Bhandari, S.; Haneef, J.; Khullar, S.; Mandal, S. *CrystEngComm,* **2014**, *16*, 8375-8389.

(16) Chattoraj, S.; Shi, L.; Chen, M.; Alhalaweh, A.; Velaga, S.; Sun, C. C. *Cryst. Growth Des.* **2014**, *14*, 3864-3874.

(17) Huang, Y.; Zhang, B.; Gao, Y.; Zhang, J.; Shi, L. *J. Pharm. Sci.* **2014**, *103*, 2330-2337.

(18) McKellar, S. C.; Kennedy, A. R.; McCloy, N. C.; McBride, E.; Florence, A. J. *Cryst. Growth Des.,* **2014**, *14*, 2422-2430.

(19) Kajanti, M. K.; Pyrhönen, S. O.; Maiche, A. G. *Eur. J. Cancer,* **1993**, *29*, 863-866.

(20) Cooke, J. W. B.; Bright, R.; Coleman, M. J.; Jenkins, K. P. *Org. Process Res. Dev.* **2001**, *5*, 383–386.

(21) Zhang, N.; Yin, Y.; Xu, S. J.; Chen, W. S. *Molecules,* **2008**, *13*, 1551–1569.

(22) Hoff, P. M.; Lassere, Y.; Pazdur, R. *Drugs* **1999**, *58*, 77–83.

(23) Ikeda, K.; Yoshisue, K.; Matsushima, E.; Nagayama, S.; Kobayashi, K.; Tyson, C. A.; Chiba, K.; Kawaguchi, Y. *Clinical Cancer Res.* **2000**, *6*, 4409-4415.

(24) Damle, B. D.; Narasimhan, N. I.; Kaul, S. *Biopharm. Drug Dispo.* **2001**, *22*, 45-52.

(25) http://www.wcrf.org/int/cancer-facts-figures/worldwide-data

(26) Ohkawa, Y.; Higashiyama, K.; Sugaya, S.; Asoh, T.; Maeda, H.; Sasaki, K.; Nakayama, T. *Biol. Pharm. Bull.* **2001**, *24*, 378-384.

(27) Arias, J. L.; López-Viota, M.; Gallardo, V.; Ruiz, M. A. *Drug. Dev. Ind. Pharm.* **2010**, *36*, 744-750.

(28) Nakai, Y.; Yamamoto, K.; Terada, K.; Uchida, T.; Shimizu, N.; Nishigaki, S. *Chem. Pharm. Bull.* **1982**, *30*, 2629-2632.

(29) Nakai, Y.; Yamamoto, K.; Terada, K.; Uchida, T.; Yamaguchi, K.; Shimizu, N. *Chem. Pharm. Bull.* **1986**, *34*, 1242-1248.

(30) Actiņš, A.; Beļakovs, S.; Orola, L.; Veidis, M. V. Latvijas Ķīmijas Žurnāls **2006**, *2*, 120–124.

(31) Uchida, T.; Yonemochi, E.; Oguchi, T.; Terada, K.; Yamamoto, K.; Nakai, Y. *Chem. Pharm. Bull.* **1993**, *41*, 1632–1635.

(32) Bobrovs, R.; Actiņš, A. *Int. J. Pharm.,* **2013**, *457*, 110-117.

(33) Needham, F.; Faber, J.; Fawcett, T. G.; Olson, D. H. *Powder Diffr.* **2006**, *21*, 245–247.

(34) Bobrovs, R.; Actiņš, A. *J. Pharm. Sci,* **2012**, *101*, 4608-4614.

(35) Bobrovs, R.; Seton, L.; Actiņš, A. *CrystEngComm,* DOI: 10.1039/C4CE01215A.

(36) A list of generally regarded as safe (GRAS) chemicals can be downloaded from http://www.accessdata.fda.gov/ scripts/fcn/fcnNavigation.cfm?rpt=eafusListing

(37) Cheney, M. L.; Shan, N.; Healey, E. R.; Hanna, M.; Wojtas, L.; Zaworotko, M. J.; Sava, V.; Song, S.; Sanchez-Ramos, J. R. *Cryst. Growth Des.* **2010**, *10,* 394-405.

(38) Cambridge Structural Database, ver. 5.33, ConQuest Version 1.16, February 2014 update; www.ccdc.cam.ac.uk.

(39) Gier, H.; Roth, W.; Schumm, S.; Gerhards, M. *J. Mol. Struct.* **2002**, *610*, 1-16.

(40) Thakuria, R.; Cherukuvada, S.; Nangia, A. *Cryst. Growth Des.* **2014**, *12,* 3944-3953.

(41) Ito, K.; Lim, S.; Caramori, G.; Cosio, B.; Chung, K. F.; Adcock, I. M. Barnes, P. J. *Proc. Nat. Acad. Sci.* **2002**, *99*, 8921-8926.

(42) Aitipamula, S.; Wong, A. B. H.; Chow, P. S.; Tan, R. B. H. *CrystEngComm* **2013**, *15*, 5877 – 5887.

(43) Clarke, H. D.; Arora, K. K.; Bass, H.; Kavuru, P.; Ong, T. T.; Pujari, T.; Wojtas, L.; Zaworotko, M. J. *Cryst. Growth Des.* **2010**, *10*, 2152-2167.

(44) Mukherjee, A.; Grobelny, P.; Thakur, T. S; Desiraju, G. R. *Cryst. Growth Des.* **2011**, *11*, 2637-2653.

(45) Karki, S.; Friscic, T.; Jones, W.; Motherwell, W. D. S. *Mol. Pharmaceutics* **2007**, *4*, 347-354.

(46) Ueto, T.; Takata, N.; Muroyama, N.; Nedu, A.; Sasaki, A.; Tanida, S.; Terada, K. *Cryst. Growth Des.* **2012**, *12*, 485-494.

(47) Aitipamula, S.; Chow, P. S.; Tan, R. B. H. *Acta Crystallogr. E* **2009**, *65*, o2126-o2127.

(48) Trask, A. V.; Motherwell, W. D. S. S.; Jones, W. *Int. J. Pharm.* **2006**, *320*, 114-123.

(49) Bučar, D. –K.; Henry, R. F.; Zhang, G. G. Z.; MacGillivray, L. R. *Cryst. Growth Des.* **2014**, *14*, 5318–5328.

(50) Elbagerma, M. A.; Edwards, H. G. M.; Munshi, T.; Hargreaves, M. D.; Matousek, P.; Scowen, I. J. *Cryst. Growth Des.* **2010**, *10*, 2360–2371.

(51) Stability testing of new drug substances and products—Q1A (R2). (ICH), International Conference on Harmonization. Originally published 1994, revised 2003.

(52) Zhu, H. J.; Yuen, C. M.; Grant, D. J. W. *Int. J. Pharm.*, **1996**, *135*, 151–160.

(53) Fagerberg, J. H.; Tsinman, O.; Sun, N.; Tsinman, K.; Avdeef, A.; Bergström, C. A. S. *Mol. Pharmaceutics*, **2010**, *7*, 1419-1430.

(54) Sanphui, P.; Goud, N. R.; Khandavilli, U. B. R.; Nangia, A.; *Cryst. Growth Des.* **2011**, *11*, 4135-4145.

(55) Azarmi, S.; Roa, w.; Löberberg, R. *Int. J. Pharm.* **2007**, *328,* 12-21.

(56) Sheldrick, G. M. *SHELXS-97 AND SHELXL-97, Programs for the Solution and Refinement of Crystal Structures;* University of Göttingen, Göttingen, Germany, **1997**.

(57) Barbour, L. J. *X-Seed, Graphical Interface to SHELX-97 and POV-Ray, a Program for Better Quality of Crystallographic Figures;* **1999**. University of Missouri-Columbia, Missouri.

Table 2. Crystallographic parameters for TG cocrystals

Compound reference	TG-NA	TG-INA	TG-4HBA	TG-PG	TG-TP hydrate
Chemical formula	$C_{14}H_{15}FN_4O_4$	$C_{14}H_{15}FN_4O_4$	$C_{15}H_{15}FN_2O_6$	$C_{14}H_{15}FN_2O_6$	$C_{15}H_{19}FN_6O_6$
Formula Mass	322.30	322.30	338.29	326.28	398.36
Crystal system	Triclinic	Triclinic	Monoclinic	Monoclinic	Triclinic
a/Å	5.0825(10)	5.2764(11)	5.1227(10)	12.609(3)	8.4887(17)
b/Å	9.7492(19)	10.181(2)	21.618(4)	11.125(2)	8.6643(17)
c/Å	15.148(3)	13.495(3)	13.215(3)	19.976(4)	12.184(2)
α/°	77.78(3)	87.43(3)	90.00	90.00	91.83(3)
β/°	89.74(3)	81.56(3)	93.39(3)	92.16(3)	100.87(3)
γ/°	77.45(3)	78.70(3)	90.00	90.00	105.30(3)
Unit cell volume/Å^3	715.4(2)	703.1(3)	1460.9(5)	2800.2(10)	845.7(3)
Temperature/K	110(2)	110(2)	110(2)	110(2)	110(2)
Space group	*P*1	*P*1	$P2_1/n$	*C*2/*c*	*P*1
No. of reflections measured	9583	9977	9224	9864	11773
No. of independent reflections	3440	3412	3487	3450	4131
R_{int}	0.0594	0.0147	0.0306	0.0160	0.0298
Final R_1 values ($I > 2\sigma(I)$)	0.0905	0.0400	0.0700	0.0500	0.0523
Final $wR(F^2)$ values ($I > 2\sigma(I)$)	0.2628	0.1117	0.1975	0.1366	0.1476
Final R_1 values (all data)	0.0964	0.0426	0.0769	0.0515	0.0555
Final $wR(F^2)$ values (all data)	0.2711	0.1200	0.2090	0.1382	0.1576

Table 3. Neutron Normalized Intermolecular Interactions in the Crystal Structures of TG cocrystals.

Crystal forms	D–H···A[a]	H···A/Å	D···A/Å	D–H···A/°	Symmetry code
TG-NA	N1–H1···N4	1.81	2.814(3)	176	1+x,-1+y,z
	N3–H2···O2	1.92	2.899(3)	162	1-x,1-y,2-z
	N3–H4···O4	2.09	3.072(3)	164	-1+x,y,z
	C3–H3···F1	2.3	3.370(3)	171	-x,-y,1-z
	C5–H5···O2	2.89	3.445(3)	112	-1+x,y,z
	C6–H6A···O2	2.51	3.074(3)	111	Intramolecular
	C6–H6A···O3	2.27	3.251(3)	150	1+x,y,z
	C7–H7A···O1	2.54	3.392(3)	135	-1+x,1+y,z
	C8–H8A···O1	2.75	3.486(4)	125	-1+x,1+y,z
	C8–H8B···F1	2.56	3.316(3)	126	-x,-y,1-z
	C13–H13···O4	2.78	3.314(3)	110	-1+x,y,z
TG-INA	N1–H1···N4	1.81	2.8140(15)	174	-x,1-y,1-z
	N3–H2···O4	1.86	2.8659(15)	176	3-x,-y,2-z
	N3–H4···O2	1.98	2.9679(14)	167	1+x,y,1+z
	C3 -H3···F1	2.31	3.3807(15)	170	1-x,1-y,1-z
	C6–H6A···N3	3.02	3.4500(16)	104	-1+x,y,-1+z
	C6–H6A···O4	2.37	3.3059(15)	144	2-x,-y,1-z
	C6–H6B···O2	2.57	3.1020(15)	109	Intramolecular
	C6–H6B···O3	2.34	3.3684(16)	158	-1+x,y,z
	C7–H7A···O1	2.66	3.4641(17)	131	-x,1-y,1-z
	C8–H8A···F1	2.55	3.3244(17)	128	1-x,1-y,1-z
	C11–H11···O1	2.57	3.3768(16)	131	-x,1-y,1-z
TG-4HBA	N1–H1···O5	1.77	2.770(2)	169	-x,-y,1-z

	O4–H2···O2	1.70	2.679(2)	175	-x,-y,1-z
	O6–H4···O1	1.77	2.745(2)	170	2+x,y,-1+z
	C6–H6A···O2	2.71	3.154(3)	104	Intramolecular
	C6–H6B···O2	2.40	3.387(3)	150	-x,-y,1-z
	C7–H7A···F1	3.01	3.419(3)	103	1/2+x,1/2-y,-1/2+z
	C7–H7B···O6	2.51	3.535(3)	158	-3/2+x,1/2-y,1/2+z
	C8–H8B···F1	2.64	3.056(3)	102	1/2+x,1/2-y,-1/2+z
	C8–H8B···O6	2.70	3.591(3)	139	-1/2+x,1/2-y,1/2+z
	C10–H10···F1	2.48	3.404(3)	142	1/2+x,1/2-y,-1/2+z
	C11–H11···F1	2.73	3.392(3)	119	3/2+x,1/2-y,-1/2+z
	C13–H13···O1	2.53	3.302(3)	127	2+x,y,-1+z
TG-PG	N1–H1···O2	1.81	2.8034(17)	169	3/2-x,1/2-y,1-z
	O4–H2···O5	2.24	2.7248(18)	109	Intramolecular
	O4–H2···O2	1.9	2.7572(17)	144	3/2-x,1/2-y,1-z
	O5–H4···O6	2.32	2.7566(17)	106	Intramolecular
	O5–H4···O6	1.88	2.8161(16)	159	2-x,y,3/2-z
	O6–H9···O1	1.85	2.7718(17)	154	3/2-x,1/2+y,3/2-z
	C3–H3···F1	2.37	3.3400(18)	148	1/2-x,1/2-y,1-z
	C5–H5···O3	2.92	3.302(2)	101	1-x,1-y,1-z
	C6–H6B···O5	2.82	3.289(2)	106	3/2-x,1/2-y,1-z
	C8–H8A···O4	2.67	3.586(2)	142	1-x,1-y,1-z
	C8–H8A···O5	2.83	3.481(2)	118	1-x,1-y,1-z
	C8–H8B···F1	2.62	3.403(2)	129	1/2-x,1/2-y,1-z
	C12–H12···F1	2.76	3.336(2)	113	1-x,y,3/2-z
TG-TP monohydrate	N1–H1···O6	1.71	2.7140(19)	174	1-x,-y,-z

N6–H2···O2	1.82	2.7289(19)	148	x,1+y,1+z
O6–H4···O4	1.75	2.7276(18)	170	1-x,1-y,1-z
O6–H9···N5	1.82	2.792(2)	169	-x,1-y,1-z
C6–H6A···F1	2.79	3.424(2)	117	2-x,-y,1-z
C7–H7B···O5	2.37	3.316(2)	145	1+x,y,z
C8–H8A···F1	2.59	3.431(2)	134	-1+x,y,z
C13–H13···O1	2.22	3.270(2)	164	-1+x,1+y,1+z
C14–H14A···O4	2.26	2.703(2)	102	Intramolecular
C15–H15A···O4	2.81	3.385(2)	113	-1+x,y,z
C15–H15A···O6	2.8	3.220(2)	103	x,y,1+z
C15–H15C···O3	2.74	3.326(2)	114	1-x,1-y,1-z

[a] D = Donor, A = Acceptor.

For Table of Contents Use Only

Crystal Engineering of Tegafur Cocrystals: Structural Analysis and Physicochemical Properties

Srinivasulu Aitipamula, Pui Shan Chow and Reginald B. H. Tan

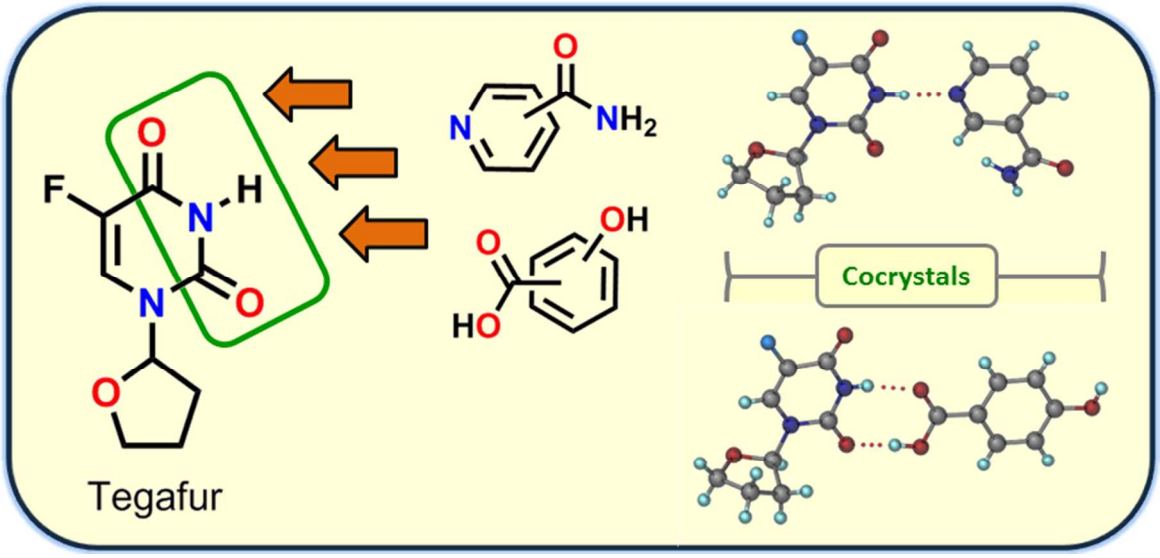

Tegafur (TG, a chemotherapy agent) suffers severe drawbacks due to non-uniform oral absorption, a short biological half-life, and poor solubility. We report five cocrystals of TG with pharmaceutically acceptable coformers. The superior stability, solubility and dissolution rate of TG-isonicotinamide cocrystal make it a promising cocrystal for development of novel TG formulations.

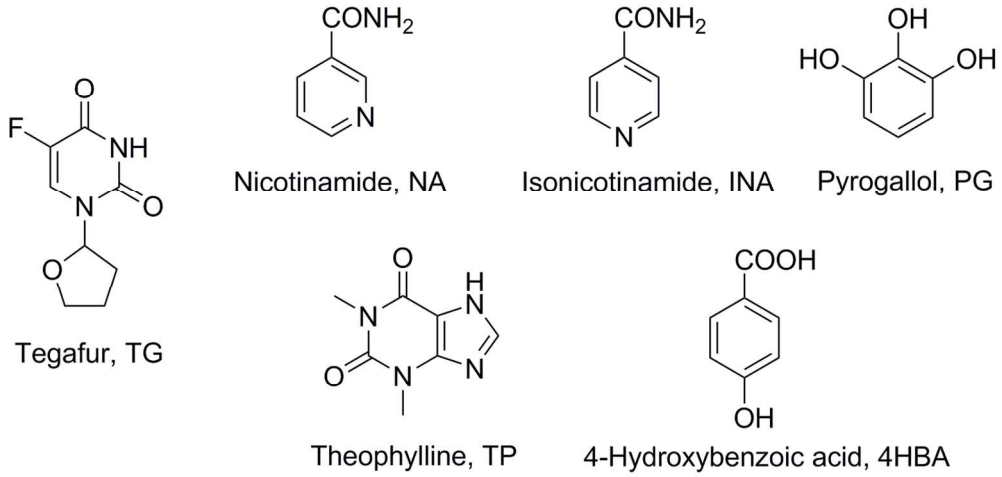

Figure 1. Molecular structure of TG and coformers that formed cocrystals reported in this paper.
128x61mm (300 x 300 DPI)

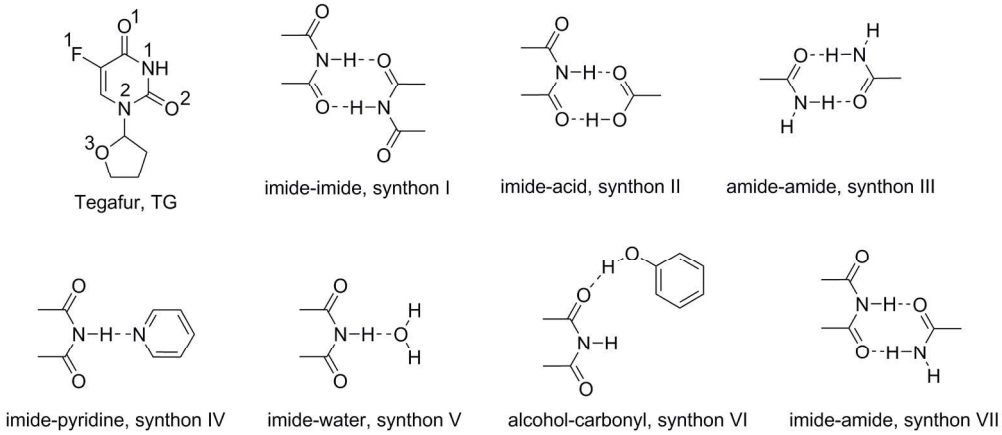

Figure 2. Some observed/plausible supramolecular synthons in the cocrystals of TG.
185x80mm (300 x 300 DPI)

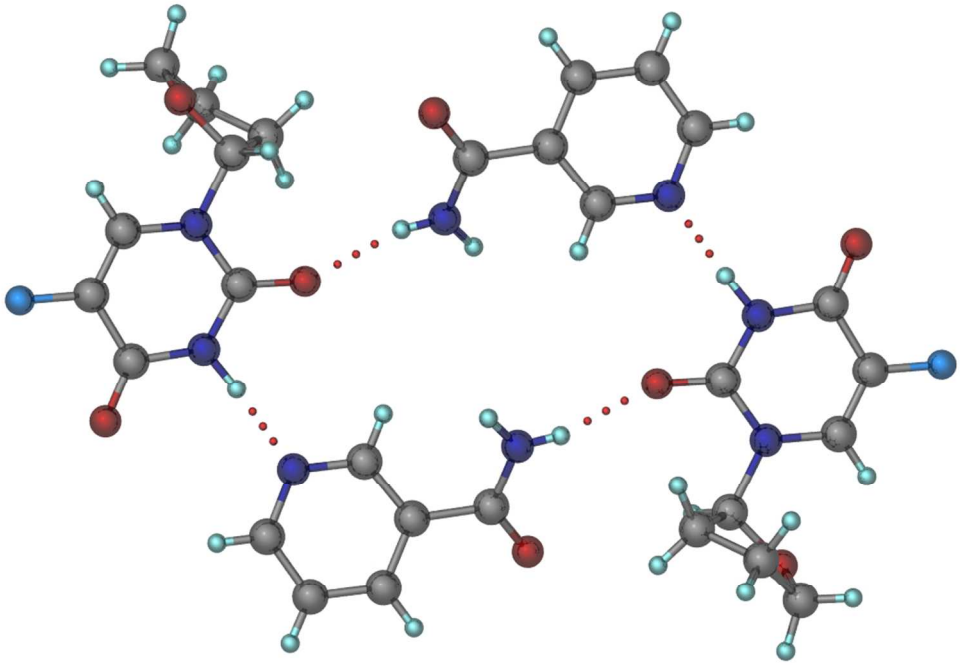

Figure 3. Crystal structure of TG-NA cocrystal, (a) a four-component hydrogen bond supramolecular unit, (b) columnar arrangement of four-component supramolecular units via N-Hamide···Oamide hydrogen bond (symmetry generated columns are shown in different colors).
287x202mm (96 x 96 DPI)

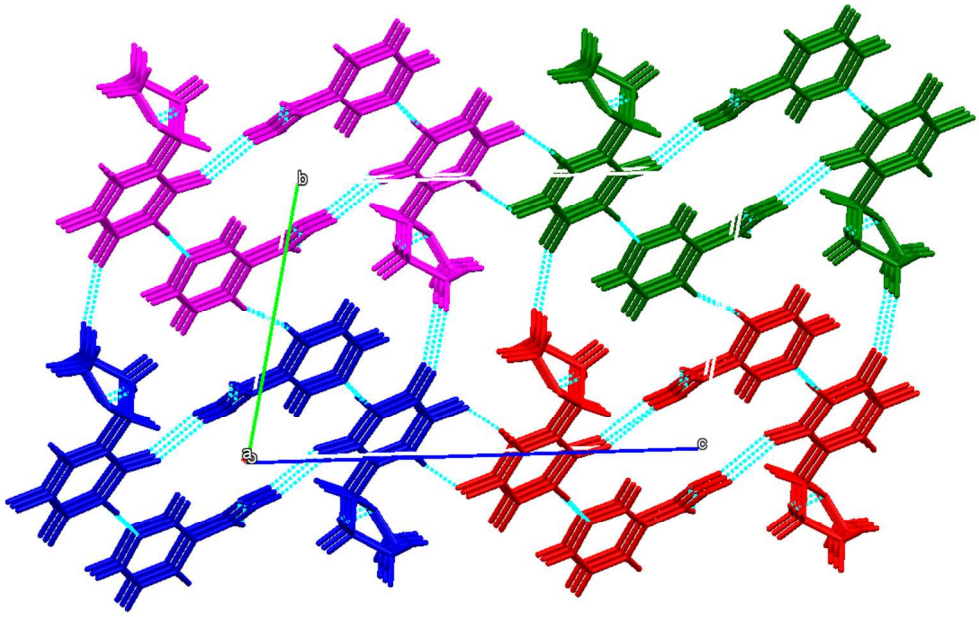

Figure 3. Crystal structure of TG-NA cocrystal, (a) a four-component hydrogen bond supramolecular unit, (b) columnar arrangement of four-component supramolecular units via N-Hamide···Oamide hydrogen bond (symmetry generated columns are shown in different colors).
294x186mm (96 x 96 DPI)

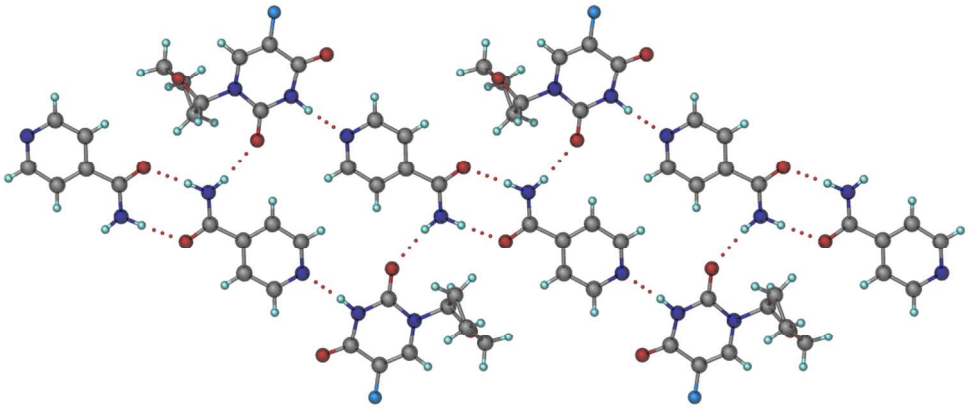

Figure 4. A part of the crystal structure of the TG-INA cocrystal. Notice the heterosynthon between TG and INA and homosynthon (synthon III) between INA molecules.
317x136mm (96 x 96 DPI)

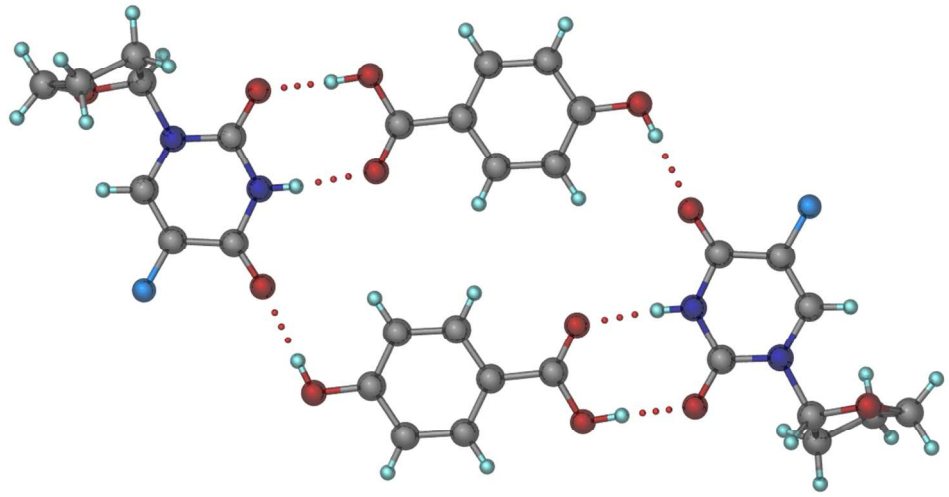

Figure 5. A four-component supramolecular unit in the crystal structure of TG-4HBA cocrystal.
317x172mm (96 x 96 DPI)

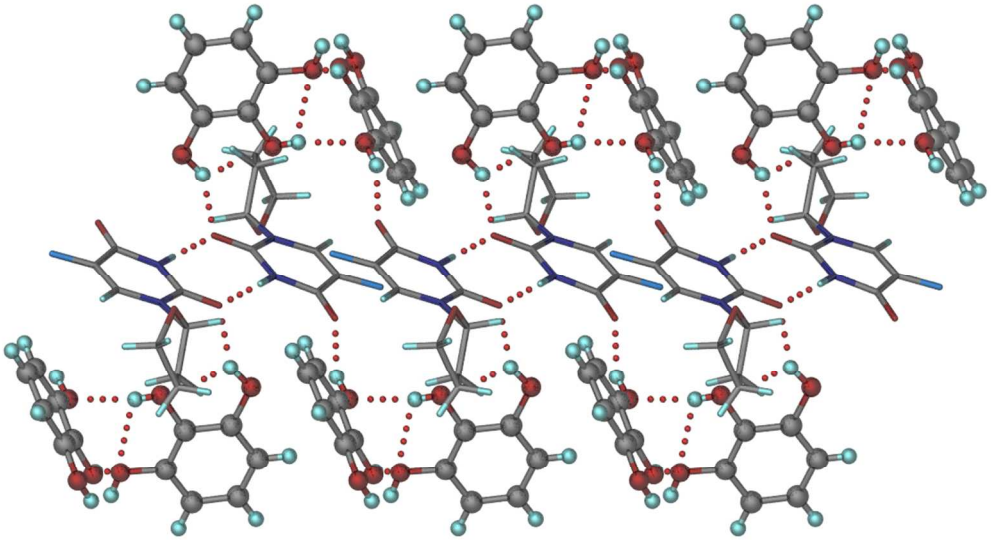

Figure 6. A part of the crystal structure of TG-PG cocrystal. Notice the dimers of TG and PG molecules mediated by homosynthons. TG molecules are shown in stick model and PG molecules are shown in ball and stick model.
297x170mm (96 x 96 DPI)

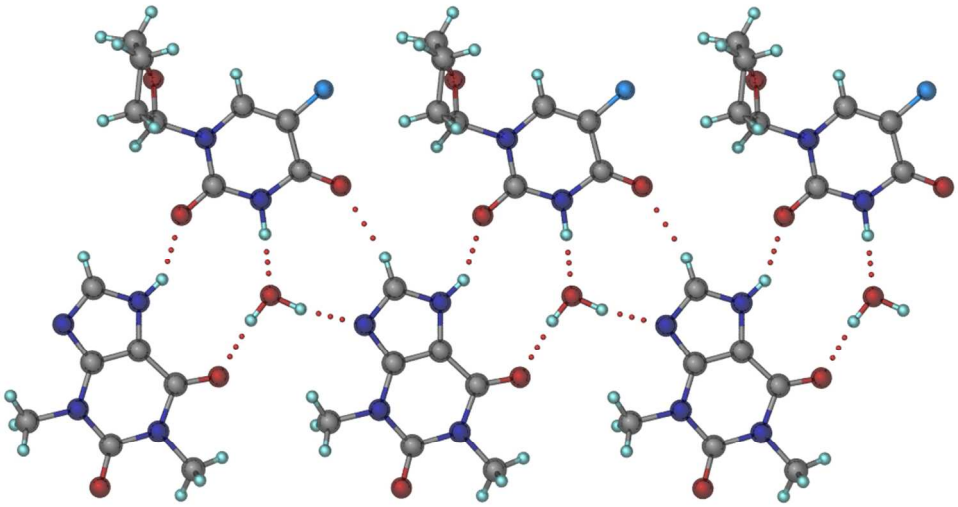

Figure 7. A part of the crystal structure of the TG-TP cocrystal hydrate.
296x162mm (96 x 96 DPI)

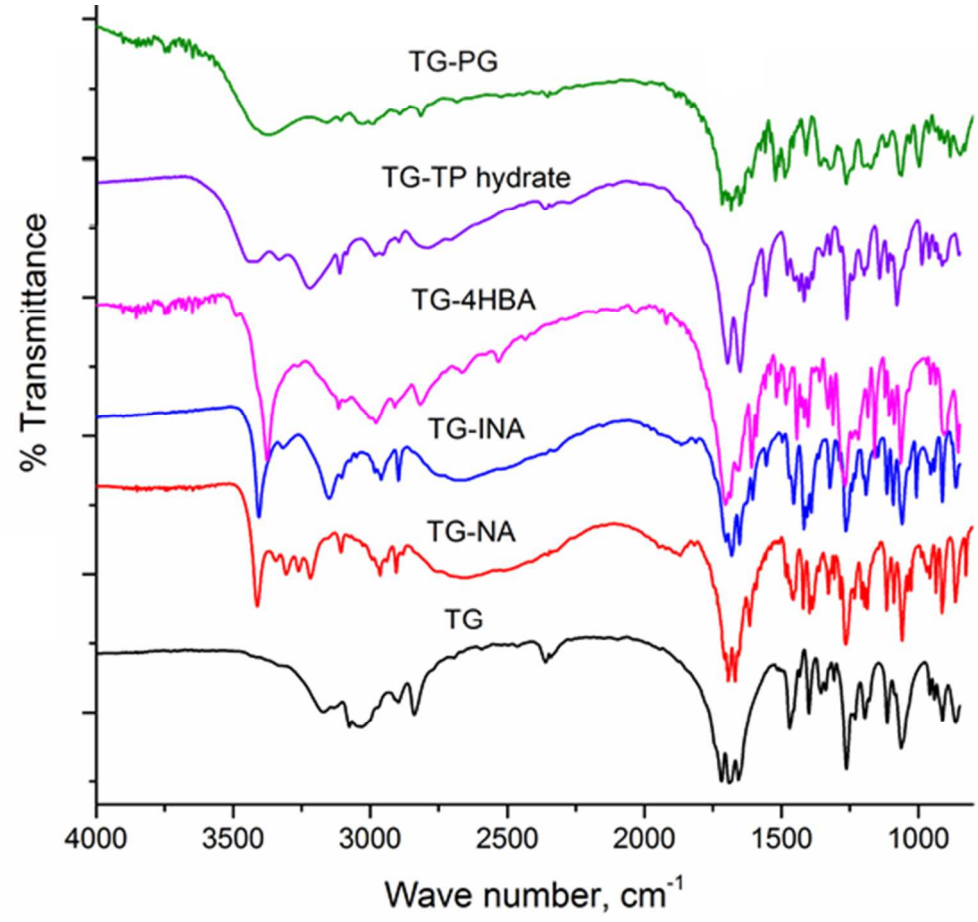

Figure 8. Comparison of the FT-IR spectra of TG and its cocrystals.
148x136mm (96 x 96 DPI)

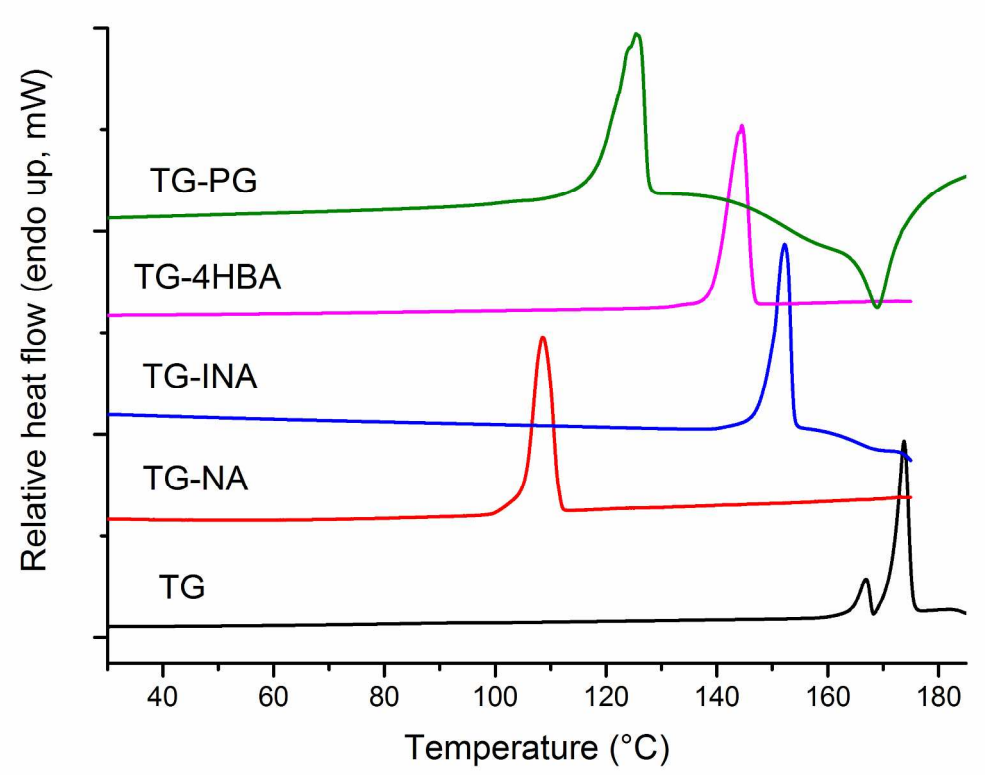

Figure 9. Thermograms of the solids reported in this paper, (a) DSC profiles of the anhydrous cocrystals, (b) TGA and DSC profile of the TG-TP cocrystal hydrate.
227x178mm (300 x 300 DPI)

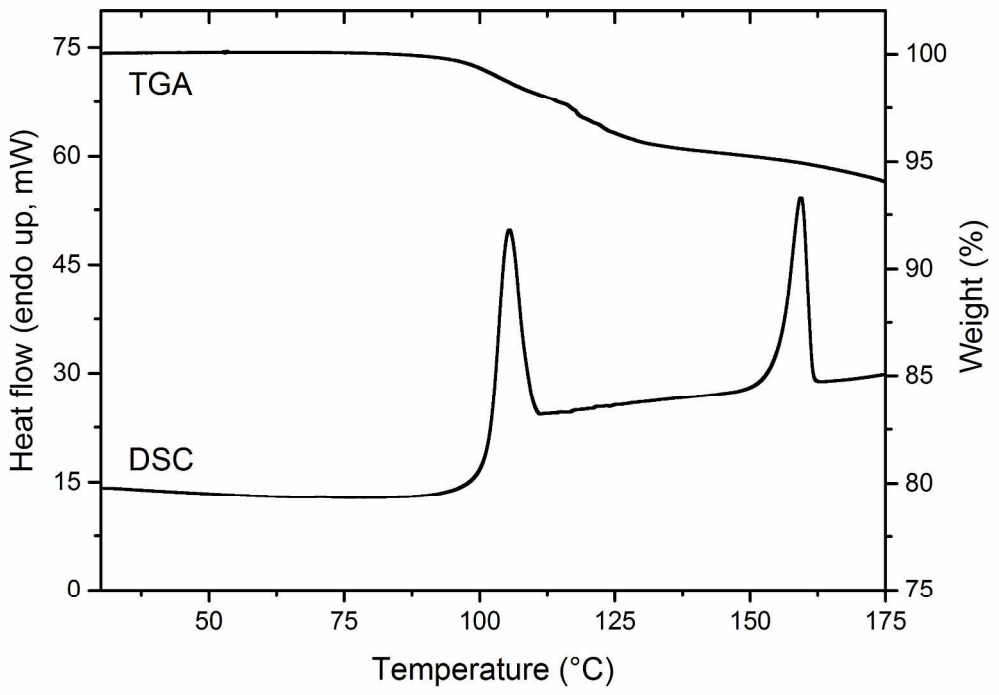

Figure 9. Thermograms of the solids reported in this paper, (a) DSC profiles of the anhydrous cocrystals, (b) TGA and DSC profile of the TG-TP cocrystal hydrate.
250x173mm (300 x 300 DPI)

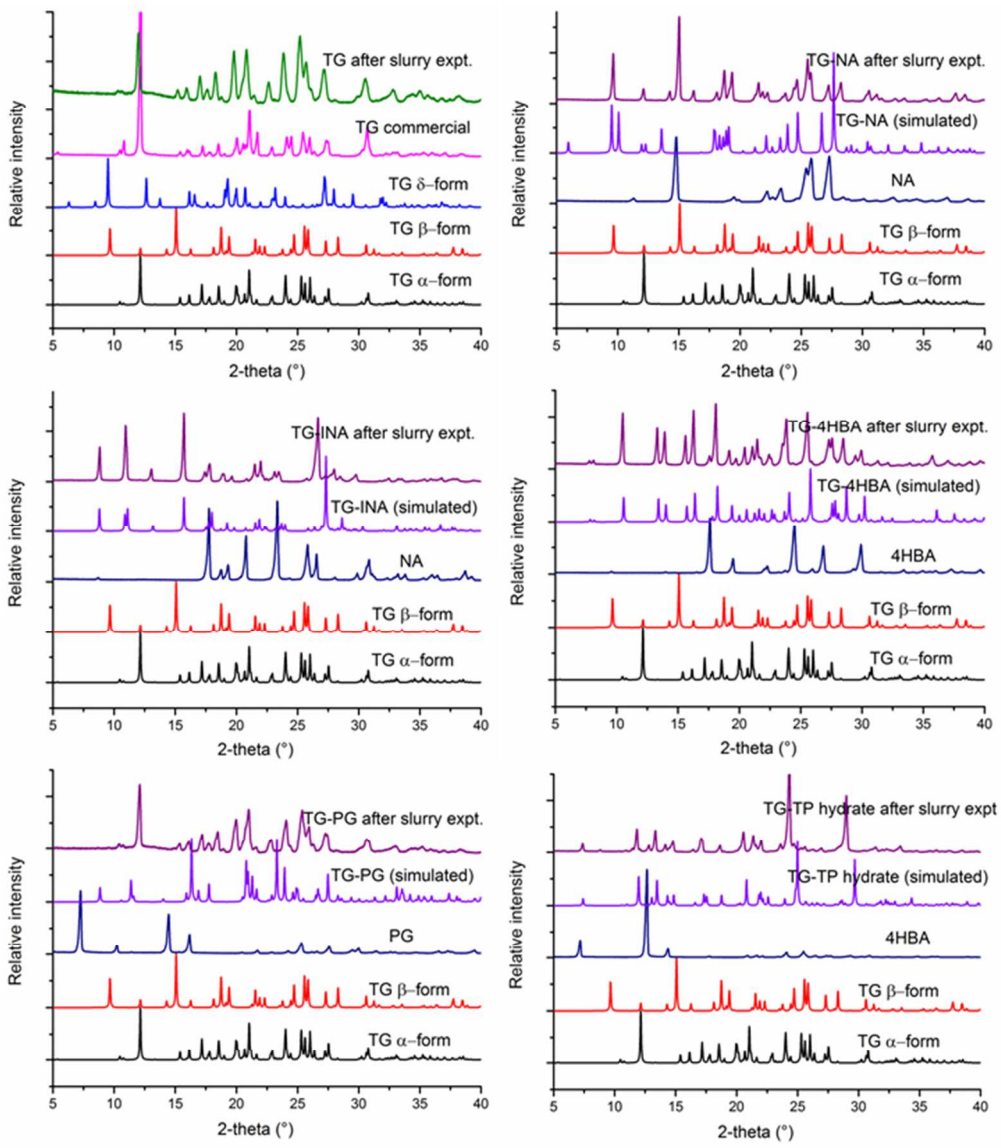

Figure 10. Overlay of PXRD patterns of the samples from slurry stability test. Notice that while TG-NA and TG-PG cocrystals dissociate and convert to β-form and α-form of TG, respectively, all other cocrystals and TG are stable under slurry conditions.
190x219mm (96 x 96 DPI)

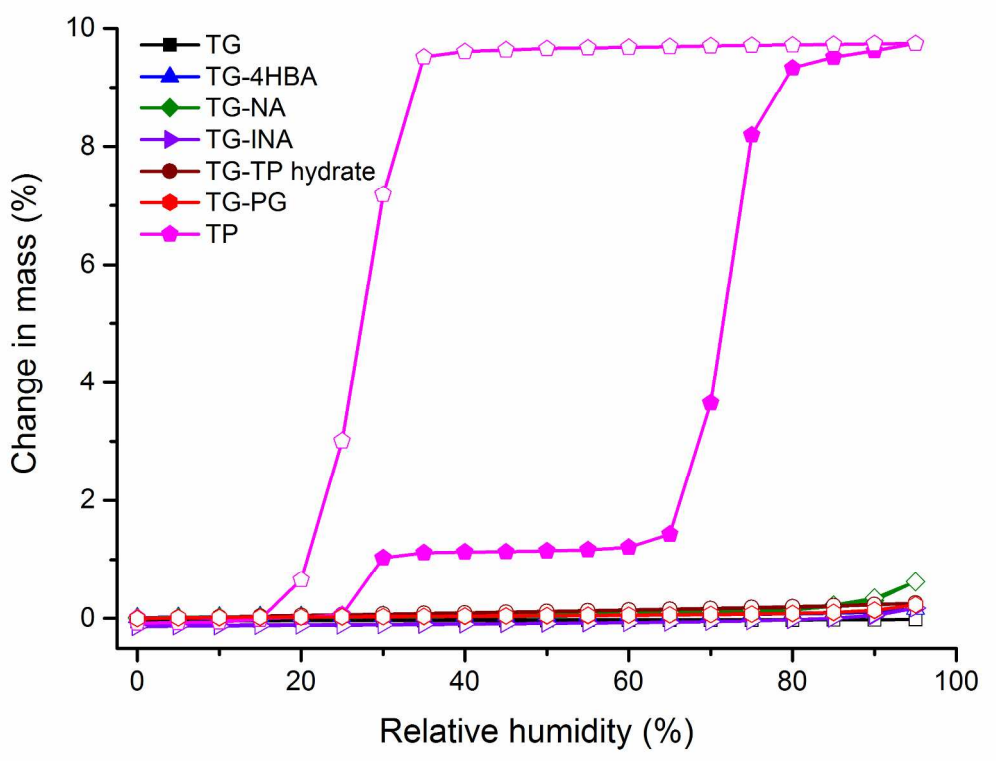

Figure 11. DVS sorption/desorption profiles of TG, TP, and the cocrystals. Profiles designated with solid and open legends correspond to sorption and desorption profiles, respectively.
233x178mm (300 x 300 DPI)

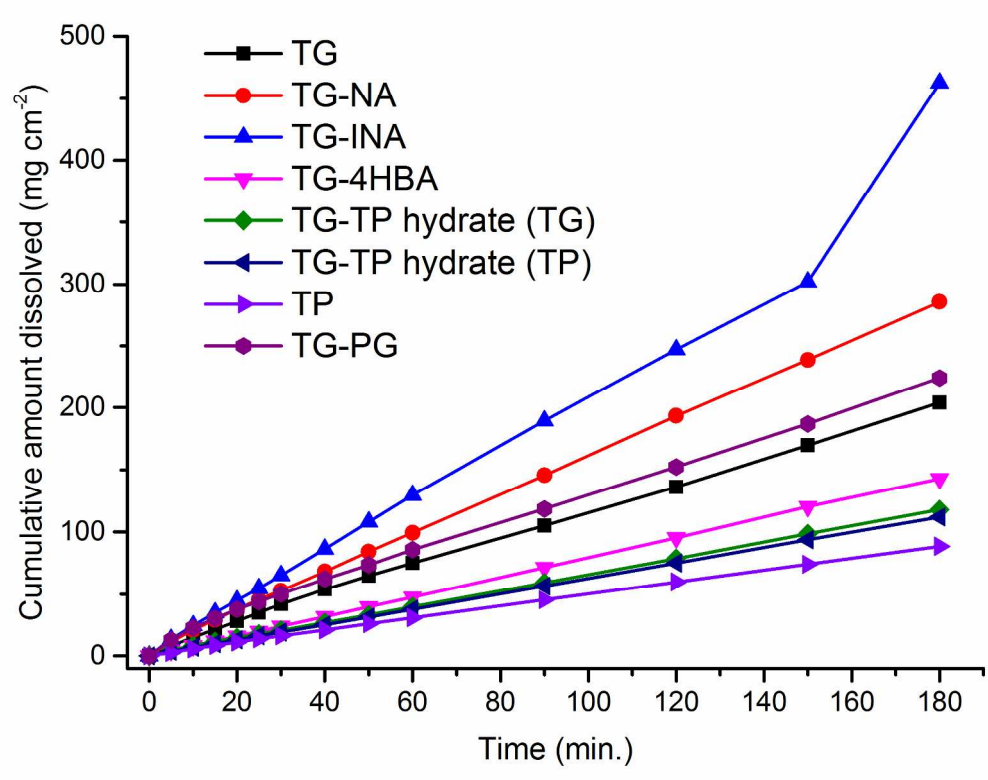

Figure 12. IDR profiles of TG, TP, and the cocrystals reported in this paper.
228x179mm (300 x 300 DPI)